SIAM J. Applied Dynamical Systems
Vol. 21, No. 4, pp. 2432–2462

On the Nonexistence of Terrestrial Canards: Linking Canards and Rivers*

Benjamin Letson† and Jonathan E. Rubin‡

Abstract. Significant past work has characterized properties of canard solutions, which spend unexpectedly long times near dynamically unstable manifolds in the phase space of an underlying dynamical system. We have recently introduced techniques to identify and analyze rivers, which are a class of trajectories that can serve as transient attractors in phase space. In this work, after generalizing the concept of rivers to arbitrary dimensions and introducing a classification of rivers, we show that maximal canards in systems with one fast and two slow variables are rivers of infinite order, or river canards. We use this relationship to provide new insights about how nearby trajectories behave and about how river canards organize the flow near the fold of a critical manifold. This analysis includes the calculation of the way-in way-out function, which provides an estimate for the extent of the delay in escape that trajectories experience when passing near the fold of a critical manifold with canard dynamics, without the need for complexification of time. We also illustrate our results for the well-known autocatalator system.

Key words. multiple timescales, local orthogonal rectification, way-in way-out function, curvature, autocatalator

MSC codes. 34C20, 34E13, 34E17, 37C10, 37C70, 37D10

DOI. 10.1137/21M1421957

1. Intro-duck-tion.

Transient phenomena have increasingly been recognized as critical to efforts to study systems across ecology [14], neuroscience [27], immunology [6], fluid dynamics [13], and other fields. Although classical dynamical systems techniques focus on long-term, asymptotic dynamics and localized transient responses to small perturbations from attracting states, the above works demonstrate that some progress on the development of methods to analyze more general forms of transient dynamics has occurred. Multiple timescale systems, which describe the interactions of variables that evolve at significantly different rates, afford a natural setting for transient dynamics to arise. Indeed, stable oscillations in fast-slow systems, sometimes called relaxation oscillations, can be thought of as compositions of transients, since they feature slow, prolonged but ultimately transient excursions in the vicinity of invariant manifolds alternating with rapid, brief, transient jumps between neighborhoods of these manifolds [16]. Special solutions called *canards* provide another source of interesting transient dynamics in some fast-slow systems. A canard also involves passage along invariant

* Received by the editors May 24, 2021; accepted for publication (in revised form) June 29, 2022; published electronically December 2, 2022.
https://doi.org/10.1137/21M1421957
Funding: This work was partially funded by NSF Awards DMS-1612913 and DMS-1951095 and an Andrew Mellon Predoctoral Fellowship from the University of Pittsburgh.
† Department of Mathematics, University of Pittsburgh, Pittsburgh, PA 15260 USA. Current address: SFL Scientific, Boston, USA (bgletson@gmail.com).
‡ Department of Mathematics, University of Pittsburgh, Pittsburgh, PA 15260 USA (jonrubin@pitt.edu).

manifolds and is distinguished as a trajectory that passes in the vicinity of a special point called a folded singularity and subsequently spends a surprisingly long time near a manifold that is dynamically unstable [17]. Canards can arise as one-time transients (e.g., [28]) or as transient segments that arise in each cycle within periodic mixed-mode oscillations [7].

Recently, we developed methods to precisely define and analyze *rivers*, which are central to another form of transient dynamics, in planar systems [20]. Loosely speaking, a river has been understood in the literature to be a trajectory that attracts nearby trajectories over some finite time window but is not related in a clear way to asymptotic attractors within the flow [10, 9, 2, 31]. Our work demonstrates that these trajectories can be identified and explained using the curvature of a flow; specifically, a river in the plane is a trajectory that has vanishing curvature and derivative of curvature at a special point, which we call the *confluence*. To derive properties of rivers in the plane, we used a coordinate transformation known as *local orthogonal rectification*, or LOR. The LOR method generalizes to systems of arbitrary dimension, and although neither rivers nor LOR require any timescale separation, we have applied LOR to the two-timescale, three-dimensional normal form for a system with a certain type of folded singularity, namely, a folded saddle-node singularity, known to give rise to canard solutions [21]. Interestingly, our analysis identified a special trajectory within the flow of this system that organizes the canard dynamics and has everywhere vanishing curvature within the coordinate frame obtained from the LOR transformation. This result suggests the possibility of a strong connection between canards and rivers, and the goal of this paper is to characterize this relationship.

To achieve this aim, we start by reminding readers of fundamental ideas associated with invariant manifolds and canards in fast-slow systems as well as the LOR transformation, in section 2. Next, in section 3, we generalize the definition of rivers to arbitrary dimensions, which also involves establishing a classification of rivers based on the order to which curvature vanishes along them. In section 4, we prove that there is a strong relationship between rivers and canards. We use this relation to analyze and explain some of the organizational properties of the associated dynamics for a normal form, with one fast and two slow variables, associated with flow near a canard point at a fold of a critical manifold and to compute the way-in way-out function that quantifies delayed escape from the manifold. To show that these results extend beyond this specific system, in section 5, we study how near identity transformations affect the curvature of flow and associated quantities. Together, these results show that all canards in this setting lie in a small neighborhood of a class of rivers. We illustrate our results in an example system, the autocatalator, in section 6, and we conclude with a brief discussion in section 7.

2. Background theory.

2.1. Invariant manifolds and canards in fast-slow systems.

Following past work [11, 35], we express the fast-slow systems of interest as

$$\dot{z} = H(z,\varepsilon) = F(z) + \varepsilon G(z,\varepsilon), \tag{2.1}$$

where $z \in \mathbb{R}^n$, functions F, G are $\mathcal{O}(1)$ in ε, and $0 < \varepsilon \ll 1$ sets the slow timescale of the system. For system (2.1), the layer problem or fast subsystem is obtained in the $\varepsilon \downarrow 0$ limit as

$$\dot{z} = F(z). \tag{2.2}$$

Moreover, a *critical manifold* can be defined from the equilibrium points of the layer system, given by $\mathcal{M} = \{z|F(z) = 0\}$. Suppose that a k-dimensional critical manifold exists, with $\text{rank}(F) = n - k$ at all $z \in \mathcal{M}$. A dynamical system, called the reduced problem or slow subsystem associated with (2.1), can be defined on $\mathcal{M}$ by applying an appropriate projection to G:

$$\dot{z} = \Pi^{\mathcal{M}} G(z, 0), \tag{2.3}$$

where $\Pi^{\mathcal{M}}$ can be defined pointwise on $z \in \mathcal{M}$ by subtracting the projection onto the orthogonal complement of the tanget space, $(T_z\mathcal{M})^{\perp}$, from the $n \times n$ identity matrix (see [35] for details).

To analyze a fast-slow system, we typically employ geometric singular perturbation theory (GSPT), which is sometimes called Fenichel theory [11]. GSPT allows us to piece together the dynamics of (2.1) for $0 < \varepsilon \ll 1$ using (2.2) and (2.3) as long as some general assumptions hold. To discuss Fenichel's fundamental results, we recall that if $\mathcal{M}$ is a k-dimensional, locally invariant manifold for (2.2) or (2.1), then $\mathcal{M}$ is *normally hyperbolic* if there are $n - k$ eigenvalues of the linearized vector field along $\mathcal{M}$ with nonzero real part. If the linearization at any point of $\mathcal{M}$ has $n - k$ eigenvalues with negative real parts, then initial conditions near $\mathcal{M}$ will approach $\mathcal{M}$ and we say that $\mathcal{M}$ is stable; if one or more eigenvalues have positive real parts, then $\mathcal{M}$ is unstable [37]. We now state results due to Fenichel, following the statement from [16].

Theorem 2.1 (Fenichel's first manifold theorem and stable manifold theorem). *Suppose that $\mathcal{M} = \{z|F(z) = 0\}$ is a normally hyperbolic manifold for (2.2). For $\varepsilon > 0$ sufficiently small, there exists a manifold $\mathcal{M}_\varepsilon$ that is diffeomorphic to $\mathcal{M}$, is $\mathcal{O}(\varepsilon)$ close to $\mathcal{M}$, and is locally invariant under (2.1). Furthermore, $\mathcal{M}_\varepsilon$ will have the same stability type as $\mathcal{M}$, and the dynamics of the flow restricted to $\mathcal{M}_\varepsilon$ will be an $\mathcal{O}(\varepsilon)$ perturbation of the slow subsystem (2.3).*

The condition that $\mathcal{M}$ is normally hyperbolic is fairly mild and is generically true; however, Fenichel's theorem will fail to hold if $\mathcal{M}$ is not normally hyperbolic. Indeed, some of the most interesting examples in GSPT arise when parts of $\mathcal{M}$ are not normally hyperbolic. For example, at a point $z \in \mathcal{M}$, where $\mathcal{M}$ is normally hyperbolic, $D_xF(z)$ is invertible for a suitably chosen coordinate set $x \in \mathbb{R}^{n-k}$, and hence $\mathcal{M}$ can be expressed as the graph of a function, say $x = h(y)$ for some h acting on coordinates $y \in \mathbb{R}^k$. The critical manifold can lose normal hyperbolicity at a fold, which is a set of points where the graph $x = h(y)$ would have an infinite derivative. Often, the stability of the critical manifold changes across folds because at least one of the eigenvalues of $D_xF(z)$ crosses through the imaginary axis.

One of the most interesting and counterintuitive features of dynamics sometimes found near folded critical manifolds are canard solutions. A canard solution is a trajectory with an initial condition near a stable branch, call it $\mathcal{M}_S$, of the critical manifold, which evolves along $\mathcal{M}_S$, reaches a neighborhood of the fold of the critical manifold, and spends a "long time" near the unstable branch of the critical manifold, $\mathcal{M}_U$. That is, we would expect, given that $\mathcal{M}_U$ is linearly unstable, that trajectories near $\mathcal{M}_U$ should leave $\mathcal{M}_U$ in logarithmic time, as some variables will grow exponentially. A canard solution, however, will linger near the unstable critical manifold for an *algebraic* period of time [17]. In section 4.2, we will provide

a novel perspective on this characteristic delay using techniques related to curvature paired with blowup coordinates applied after the LOR transformation, which is defined in the next subsection.

A special case of (2.1) that is often considered features an explicit separation of the variables x and y as follows:

$$\begin{aligned} \dot{x} &= F(x,y), \\ \dot{y} &= \varepsilon G(x,y), \end{aligned} \tag{2.4}$$

where $x \in \mathbb{R}^{n-k}, y \in \mathbb{R}^k$ for $0 < k < n$ [1]. Here, the x variables are called the fast variables while the y variables are called the slow variables.

2.2. LOR in arbitrary dimensions. Following [21], consider an ODE and initial condition

$$\dot{x} = f(x), \qquad x(0) = x_0 \in \Omega, \tag{2.5}$$

where $f \in \mathscr{C}^r(\Omega, \mathbb{R}^n)$ for $n, r \geq 1$ and Ω is an open subset of $\mathbb{R}^n$, which induces a flow $\Phi : \Omega \times \mathbb{R} \to \Omega$. For simplicity, we introduce the notation $\partial_i = \partial/\partial\eta_i$. Suppose that $\mathcal{M}$ is a codimension-k $\mathscr{C}^s$-regular manifold embedded in Ω. Specifically, suppose there exist an indexing set A and an atlas of charts $\{(\mathcal{U}_\alpha, \sigma_\alpha)\}_{\alpha \in A}$, where $\mathcal{M} = \cup_{\alpha \in A} \sigma_\alpha(\mathcal{U}_\alpha)$, such that for all $\alpha, \beta \in A$,

1. each $\mathcal{U}_\alpha \subseteq \mathbb{R}^{n-k}$ is open with corresponding $\sigma_\alpha \in \mathscr{C}^s(\mathcal{U}_\alpha, \Omega)$ a homeomorphism on its image;
2. if $\sigma_\alpha(\mathcal{U}_\alpha) \cap \sigma_\beta(\mathcal{U}_\beta) \neq \emptyset$, then the map $\kappa_{\alpha,\beta} : U_\alpha \cap \sigma_\alpha^{-1} \circ \sigma_\beta(\mathcal{U}_\beta) \to \mathcal{U}_\beta \cap \sigma_\beta^{-1} \circ \sigma_\alpha(\mathcal{U}_\alpha)$ defined by $\kappa_{\alpha,\beta} = \sigma_\beta^{-1} \circ \sigma_\alpha$ is a diffeomorphism;
3. for all $\eta \in \mathcal{U}_\alpha$,
$$\text{dimspan}\,\{\partial_1\sigma_\alpha, \ldots, \partial_{n-k}\sigma_\alpha\} = n - k;$$
4. $\mathcal{M}$ can be equipped with a local normal frame; that is, there are mappings $N_j\sigma_\alpha \in \mathscr{C}^1(\mathcal{U}_\alpha, \mathbb{R}^n), j = 1, \ldots, k$, such that
$$\langle N_{j_1}\sigma_\alpha(\eta), v\rangle = 0,\ \langle N_{j_1}\sigma_\alpha(\eta), N_{j_2}\sigma_\alpha(\eta)\rangle = \delta_{j_1,j_2}\ \ \forall \eta \in \mathcal{U}_\alpha\ \forall v \in T_{\sigma_\alpha(\eta)}\mathcal{M},$$
where $\langle \cdot, \cdot \rangle$ denotes the standard Euclidean inner product, $j_1, j_2 \in \{1, \ldots, k\}$, and δ_{j_1,j_2} is the Kronecker delta.

We call these four conditions the *LOR assumptions*. These assumptions are quite natural for a wide range of dynamical systems. For systems of the forms (2.1) and (2.4), $\mathcal{M}$ could naturally be taken to be a critical manifold but other Riemannian manifolds could also be used. The LOR assumptions guarantee that the tangent space to $\mathcal{M}$ at any point $p \in \mathcal{M}$, denoted by $T_p\mathcal{M}$, is an n-k dimensional space. The set $\{N_j\sigma_\alpha(\eta)\}_{j=1}^k$ forms an orthonormal basis of $(T_{\sigma_\alpha(\eta)}\mathcal{M})^\perp$ on $\mathcal{U}_\alpha$. The existence of such a basis is straightforward to establish locally, and by refining our domains $\mathcal{U}_\alpha$ we can guarantee that such mappings exist. For fast-slow systems with critical manifold $\mathcal{M}$, we also note that there is a natural isomorphism between trajectories of the fast subsystem (2.2) and the normal directions over normally hyperbolic parts of $\mathcal{M}$.

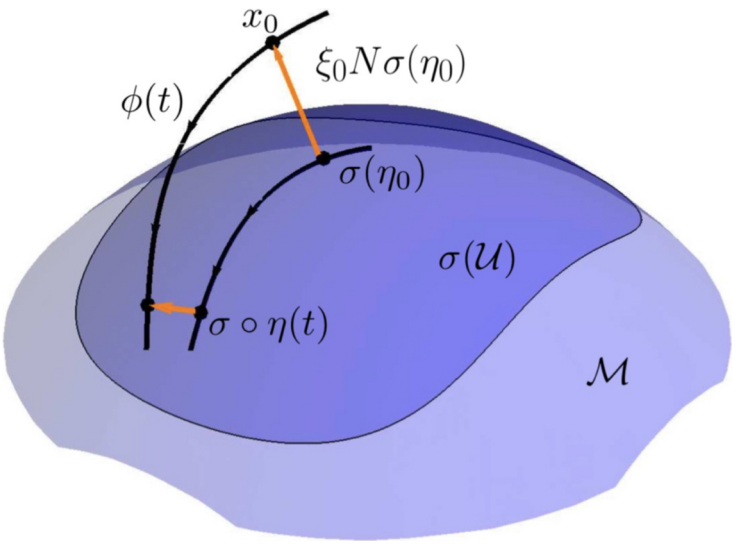

Figure 1. *An illustration of the general setup for LOR. The initial point x_0, such that $\phi(0) = x_0$, is decomposed as in (2.6), although here we drop the α subscripts. This decomposition is continued along $\phi(t)$ with (η, ξ) satisfying (2.7). This figure is adapted from [21].*

Although the next steps are also done for arbitrary k elsewhere [21], in the next section we will focus on codimension-1 manifolds, so for the moment we restrict to $k = 1$ and write $N\sigma_\alpha(\eta)$ in place of $N_1\sigma_\alpha(\eta)$. Now, suppose that we are interested in studying the dynamics near a point $x_0 \in \Omega$ that lies close to our embedded manifold. Furthermore, suppose that x_0 can be written in the form

$$x_0 = \sigma_\alpha(\eta_0) + \xi_0 N\sigma_\alpha(\eta_0), \qquad \eta_0 \in \mathcal{U}_\alpha, \quad \xi_0 \in \mathbb{R}. \tag{2.6}$$

To write (2.6), we have assumed that x_0 can be decomposed into a point on $\mathcal{M}$, namely, $\sigma_\alpha(\eta_0)$, and a vector in the orthogonal complement of $T_{\sigma_\alpha(\eta_0)}\mathcal{M}$, namely, $\xi_0 N\sigma_\alpha(\eta_0)$; see Figure 1. Past work [21] established that such a decomposition is generic, sufficiently close to $\mathcal{M}$. We define $\Psi_\alpha : \mathcal{U}_\alpha \times \mathbb{R} \to \mathbb{R}^n$ by $\Psi_\alpha(\eta, \xi) = \sigma_\alpha(\eta) + \xi N\sigma_\alpha(\eta)$ so that (2.6) can be more succinctly expressed as $x_0 = \Psi_\alpha(\eta_0, \xi_0)$.

Now, denote by $\phi(t)$ the trajectory of (2.5) such that $\phi(0) = x_0$. We want to continue tracking $\phi(t)$ in our decomposition. To do so, we seek smooth $\eta : (-\delta, \delta) \to \mathcal{U}_\alpha$, $\xi : (-\delta, \delta) \to \mathbb{R}$, which we call the *LOR coordinates* for the base manifold $\mathcal{M}$, such that $\phi(t) = \Psi(\eta(t), \xi(t))$ for $t \in (-\delta, \delta)$. Under the LOR assumptions, this continuation can be achieved and a system of ODEs that govern the evolution of $\eta(t), \xi(t)$, the *LOR equations* [21], can be derived. The LOR equations for $k = 1$ take the form

$$\begin{aligned} \dot{\eta} &= [S_\sigma(\eta, \xi)]^{-1} T f(\eta, \xi), \\ \dot{\xi} &= \langle f \circ \Psi(\eta, \xi), N\sigma(\eta) \rangle =: g(\eta, \xi), \end{aligned} \tag{2.7}$$

where

$$Tf(\eta,\xi) = \begin{pmatrix} \langle f \circ \Psi(\eta,\xi), \partial_1 \sigma(\eta)\rangle \\ \vdots \\ \langle f \circ \Psi(\eta,\xi), \partial_{n-1}\sigma(\eta)\rangle \end{pmatrix}.$$

The matrix $S_\sigma(\eta,\xi) \in \mathbb{R}^{(n-1)\times(n-1)}$ takes tangent vectors in $T_{\sigma(\eta)}\mathcal{U}_\alpha$ and exchanges them for other tangent vectors in $T_{\sigma(\eta)}\mathcal{M}$ and has as its i,j entry

$$(S_\sigma(\eta,\xi))_{i,j} = \langle \partial_i\sigma(\eta), \partial_j\sigma(\eta)\rangle + \langle \partial_i\sigma(\eta), \partial_j N\sigma(\eta)\rangle\xi.$$

We will also write system (2.7) as $\begin{pmatrix} d\eta/dt \\ d\xi/dt \end{pmatrix} = \mathcal{L}f(\eta,\xi)$. Finally, we note that for invariant curves on the tangent manifold, a simplification occurs.

Lemma 2.2. *If $\Gamma(\eta)$ is an invariant curve on $T_{\sigma(\eta)}\mathcal{M}$, then $Nf(\eta,0) = 0$, where*

$$Nf(\eta,\xi) = \begin{pmatrix} \langle f \circ \Psi(\eta,\xi), N_1\Gamma(\eta)\rangle \\ \vdots \\ \langle f \circ \Psi(\eta,\xi), N_k\Gamma(\eta)\rangle \end{pmatrix} \tag{2.8}$$

for general k and, in the notation above, $Nf(\eta,\xi) = \langle f \circ \Psi(\eta,\xi), N\Gamma(\eta)\rangle$ for $k = 1$.

3. Generalized river theory: Rivers in arbitrary dimensions. In this section, we generalize the definition of a river from planar systems, where it was recently established [20], to arbitrary dimensions. In the planar case, we have shown that rivers can help organize transient dynamics that trajectories exhibit as they approach an attractor, such as an asymptotically stable periodic orbit. Mathematically, a river in the plane is a trajectory emanating from a point where the flow has vanishing curvature and torsion. We will now use this idea along with natural equivalent conditions to generalize our definitions and to develop a new classification of rivers, which will be useful for linking rivers with canards.

Given a curve $\gamma \in \mathscr{C}^{n+2}(I,\mathbb{R}^n)$ for $I \subset \mathbb{R}$, the Frenet curvature of γ is given by

$$\kappa_\gamma(\eta) = \frac{\gamma'(\eta) \wedge \cdots \wedge \gamma^{(n)}(\eta)}{\alpha(\gamma'(\eta),\ldots,\gamma^{(n)}(\eta))},$$

where $\cdot' = d\cdot/d\eta$ and α is a certain smooth, nonzero function [19]. Therefore, for an autonomous system of ODEs $\dot{x} \equiv dx/dt = f(x)$, $f \in \mathscr{C}^{n+2}$ on a phase space $\Omega \subset \mathbb{R}^n$, an analogous curvature of the vector field f can be defined by

$$\kappa(x) := \frac{f^{(1)}(x) \wedge \cdots \wedge f^{(n)}(x)}{\alpha(f^{(1)}(x),\ldots,f^{(n)}(x))},$$

where $f^{(n)}(x) = [D_x f^{(n-1)}(x)]f(x)$ for $n \geq 2$ and $f^{(1)}(x) = f(x)$. We can apply this definition directly to compute κ_ϕ at any point along any trajectory ϕ, with parameterization supplied by the independent variable $t \in \mathbb{R}$.

We will again be most interested in the set of zero curvature, $\{\kappa(x) = 0\}$, which we call the zero-curvature locus (ZCL). Specifically, we are interested in analyzing how the ZCL organizes the phase space Ω. For convienence and later use, we define

$$\Delta_{(i_1,i_2,\ldots,i_n)} f(x) := f^{(i_1)}(x) \wedge f^{(i_2)}(x) \wedge \cdots \wedge f^{(i_n)}(x) \tag{3.1}$$

for $i_1, i_2, \ldots, i_n \in \{1, \cdots, n+2\}$. Clearly $\kappa(x) = 0$ if and only if $\Delta_{(1,2,\ldots,n)} f(x) = 0$.

Generically, the ZCL will be a codimension-one manifold embedded in Ω, which we denote by $\mathcal{Z}$. To study how the flow Φ behaves near the ZCL, we will parameterize a patch of $\mathcal{Z}$ using a chart $\sigma : \mathcal{U} \subseteq \mathbb{R}^{n-1} \to \Omega$ and we will use LOR to analyze the local dynamics. Note that, because σ provides a parameterization of a level set of the curvature function, we can choose

$$N\sigma(\eta) = \frac{\nabla\kappa \circ \sigma(\eta)}{\|\nabla\kappa \circ \sigma(\eta)\|}$$

as a normal vector to our chart.

Note that in the (η, ξ) LOR frame with base manifold $\mathcal{Z}$, σ corresponds to $\{\xi = 0\}$. Correspondingly, referring to system (2.7), the manifold $\mathcal{Z}$ is locally invariant on a subpatch $\sigma(\mathcal{U}') \subset \sigma(\mathcal{U})$ if and only if $g(\eta, 0) = 0$ for all $\eta \in \text{int } \mathcal{U}'$, or

$$\langle f \circ \sigma(\eta), N\sigma(\eta) \rangle = 0 \qquad \forall\, \eta \in \text{int } \mathcal{U}'. \tag{3.2}$$

Thus, the manifold $\mathcal{Z}$ is best aligned with the flow for those η values for which $g(\eta, 0) = 0$, which motivates the following definition.

Definition 3.1. *A confluence is a point η such that $g(\eta, 0) = 0$ and the confluence set corresponding to $(\mathcal{U}, \sigma)$ is the set $C_\sigma = \{\eta | g(\eta, 0) = 0\}$.*

Note that C_σ defines a collection of points $(\eta, 0)$ from $\mathcal{Z}$ that need not form an invariant set, except in the special case that it includes all of $\mathcal{Z}$.

Definition 3.2. *Given an atlas (i.e., collection of charts) $\{(\mathcal{U}_\beta, \sigma_\beta)\}_{\beta \in B}$ of $\mathcal{Z}$, we define the confluence set for $\mathcal{Z}$ by*

$$C_{\mathcal{Z}} = \bigcup_{\beta \in B} C_{\sigma_\beta}.$$

Definition 3.3. *A river is a trajectory ϕ such that $\phi(0) \in C_{\mathcal{Z}}$.*

Note that computing an atlas for $\mathcal{Z}$ may be a nontrivial task, so we next present a chart-free equivalent condition to membership in the confluence set defined in Definition 3.2, which is computationally efficient and also explicitly connects rivers to curvature.

Theorem 3.4. *The following are equivalent:*

(C1) *$x \in \Omega$ is a confluence.*
(C2) *$\Delta_{(1,\ldots,n-1,n)} f(x) = \Delta_{(1,\ldots,n-1,n+1)} f(x) = 0$.*
(C3) *The trajectory ϕ such that $\phi(0) = x$ satisfies*

$$\kappa_\phi(0) = \frac{d\kappa_\phi}{dt}(0) = 0.$$

Proof. Suppose that $x \in C_{\mathcal{Z}}$. Thus, $\kappa(x) = 0$ and $\langle f(x), \nabla\kappa(x)\rangle = 0$. Now, let ϕ be the trajectory such that $\phi(0) = x$. We have $\kappa_\phi(0) = \kappa \circ \phi(0) = 0$ and

$$0 = \langle f \circ \phi(t), \nabla\kappa \circ \phi(t)\rangle\Big|_{t=0} = \frac{d}{dt}\kappa \circ \phi(t)\Big|_{t=0} = \frac{d\kappa_\phi}{dt}(0),$$

where we have used the chain rule and the definition of $\kappa(x)$, respectively. Thus we have shown that (C1) implies (C3), and as the relations used are equalities, we have also shown that (C3) imples (C1).

From the definition of κ_ϕ, differentiation yields

$$\begin{aligned}\frac{d\kappa_\phi}{dt}(t) &= \frac{d}{dt}\left(\frac{\dot\phi(t) \wedge \cdots \wedge \phi^{(n)}(t)}{\alpha(\dot\phi(t), \ldots, \phi^{(n)}(t))}\right)\\ &= \frac{1}{\alpha(\dot\phi(t), \ldots, \phi^{(n)}(t))} \times \\ &\quad \left(\frac{d}{dt}\dot\phi(t) \wedge \cdots \wedge \phi^{(n)}(t) - \frac{\dot\phi(t) \wedge \cdots \wedge \phi^{(n)}(t)}{\alpha(\dot\phi(t), \cdots, \phi^{(n)}(t))}\frac{d}{dt}\alpha(\dot\phi(t), \cdots, \phi^{(n)}(t))\right).\end{aligned} \tag{3.3}$$

Note that at $t = 0$, $\dot\phi(0) \wedge \cdots \wedge \phi^{(n)}(0) = 0$ and therefore the $d\alpha/dt$ term in (3.3) will vanish. Hence, we need only compute the derivative of the wedge product. Based on the multilinearity of the wedge product and the Δ notation from (3.1), we can write this expression as

$$\frac{d}{dt}\dot\phi \wedge \cdots \wedge \phi^{(n)} = \sum_{j=1}^{n} \Delta_{(1,\ldots,n)+e_j} f \circ \phi(t), \tag{3.4}$$

where e_j is the jth canonical basis vector. For $1 \le j \le n-1$, the indices in all but the last term in the above sum have a repeated index, e.g., $(2, 2, 3, \ldots, n), (1, 3, 3, \ldots, n)$, and so on; the corresponding wedge products are zero, as repeated vectors in a determinant are obviously collinear. Hence (3.4) reduces to

$$\frac{d}{dt}\dot\phi \wedge \cdots \wedge \phi^{(n)} = \dot\phi \wedge \ddot\phi \wedge \cdots \wedge \phi^{(n-1)} \wedge \phi^{(n+1)}$$

and thus $\kappa_\phi(0) = d\kappa_\phi/dt(0) = 0$ is equivalent to $\Delta_{1,2,\ldots,n-1,n} f(x) = \Delta_{1,2,\cdots,n-1,n+1} f(x) = 0$. Therefore we have shown that conditions (C2) and (C3) are equivalent, and hence (C1) and (C2) are equivalent as well. ∎

Theorem 3.4 provides an obvious corollary that can be used to compute $C_{\mathcal{Z}}$.

Corollary 3.5.

$$C_{\mathcal{Z}} = \{\Delta_{(1,\ldots,n-1,n)} f(x) = 0\} \cap \{\Delta_{(1,\ldots,n-1,n+1)} f(x) = 0\}.$$

Corollary 3.5 provides a way to compute $C_{\mathcal{Z}}$ that is chart-independent and hence is much more efficient than using the condition derived directly from invariance of $\mathcal{Z}$.

A confluence is a point where the ZCL is well aligned with the flow (Definition 3.1), and the order of this alignment indicates how this alignment will persist, and hence the extent to

which trajectories will stay near the ZCL, as the flow evolves beyond the confluence; thus, we use the order of alignment as a measure of the strength of a river. Note that for a river ϕ, we can write

$$\kappa_\phi(t) = \frac{d^2\kappa_\phi}{dt^2}(0)t^2 + \mathcal{O}(t^3)$$

for small t. Thus, this measure of the strength of ϕ should be inversely proportional to $|d^2\kappa_\phi/dt^2(0)|$. This observation leads us to a classification of rivers.

Definition 3.6. *A trajectory ϕ is a class k river if*

$$\frac{d\kappa_\phi}{dt}(0) = \frac{d^2\kappa_\phi}{dt^2}(0) = \cdots = \frac{d^k\kappa_\phi}{dt^k}(0) = 0.$$

Clearly, every river is at least class 1. We can translate the condition from Definition 3.6 into one involving the Δ notation from (3.1) after we establish some combinatorial notation.

Definition 3.7. *Let $\mathscr{L}_0 = \{(1,\dots,n)\}$. Using power set notation, define $G : 2^{\mathbb{N}_+^n} \to 2^{\mathbb{N}_+^n}, B : \mathbb{N}_+^n \to \mathbb{N}_+^n$ as follows, where S is any collection of subsets of $\mathbb{N}_+^n$:*

$$G(S) = \bigcup_{\substack{s\in S\\ j\in\{1,\dots,n\}}} s + e_j$$

$$B(s_1, s_2, \dots, s_n) = \begin{cases} (s_1, s_2, \dots, s_n) & s_i \neq s_j \text{ for all } 1 \le i < j \le n, \\ \emptyset & \text{otherwise}, \end{cases} \tag{3.5}$$

and let $B(S) = \cup_{s\in S} B(s)$. Finally, define $\mathscr{L}_k = B \circ G(\mathscr{L}_{k-1})$ for $k > 0$. For convenience, we denote $\mathscr{L} = \cup_{k\ge 0}\mathscr{L}_k$.

Intuitively, G adds every canonical basis vector to each element of a set of positive integer vectors of length n and B deletes any of the resulting vectors that features a repeated entry. For example,

$$\begin{aligned} G(\mathscr{L}_0) &= \{(2,2,3,\dots,n),(1,3,3,\dots,n),\dots,(1,2,3,\dots,n-2,n,n),\\ &\quad (1,2,3,\dots,n-1,n+1)\},\\ \mathscr{L}_1 &= B\circ G(\mathscr{L}_0) = \{(1,2,3,\dots,n-1,n+1)\},\\ G(\mathscr{L}_1) &= \{(2,2,3,\dots,n-1,n+1),(1,3,3,\dots,n-1,n+1),\dots,\\ &\quad (1,2,3,\dots,n-2,n,n+1),(1,2,3,\dots,n-2,n-1,n+2)\}, \text{ and}\\ \mathscr{L}_2 &= B\circ G(\mathscr{L}_1) = \{(1,2,3,\dots,n-2,n,n+1),(1,2,3,\dots,n-2,n-1,n+2)\}. \end{aligned}$$

With this notation established, we provide an efficient way to identify class k rivers.

Theorem 3.8. *A trajectory ϕ is a class k river if and only if $x = \phi(0)$ satisfies*

$$\sum_{\ell\in\mathscr{L}_i} \Delta_\ell f(x) = 0 \qquad \forall i \in \{0,\dots,k\}.$$

Before proving this theorem, we prove a helpful computational lemma.

Lemma 3.9. *Suppressing time dependence,*

$$\frac{d^i}{dt^i}\dot{\phi}\wedge\cdots\wedge\phi^{(n)}=\sum_{\ell\in\mathscr{L}_i}\Delta_\ell f\circ\phi.$$

Proof. Note that $\mathscr{L}_1=\{(1,\dots,n-1,n+1)\}$, hence we have already shown the $i=1$ case within the proof of Theorem 3.4. If the desired equality holds at the ith level, then differentiation yields

$$\frac{d^{i+1}}{dt^{i+1}}\dot{\phi}\wedge\cdots\wedge\phi^{(n)}=\frac{d}{dt}\sum_{\ell\in\mathscr{L}_i}\Delta_\ell f\circ\phi.$$

Expanding, we obtain

$$\frac{d}{dt}\sum_{\ell\in\mathscr{L}_i}\Delta_\ell f\circ\phi=\frac{d}{dt}\sum_{\ell\in\mathscr{L}_i}\phi^{(\ell_1)}\wedge\cdots\wedge\phi^{(\ell_n)}=\sum_{\substack{\ell\in\mathscr{L}_i\\ j\in\{1,\cdots,n\}}}\phi^{(\ell_1+\delta_{1,j})}\wedge\cdots\wedge\phi^{(\ell_n+\delta_{n,j})},$$

where $\delta_{i,j}$ denotes the Kronecker delta function. Collecting terms and using our definition of G gives

$$\sum_{\substack{\ell\in\mathscr{L}_i\\ j\in\{1,\cdots,n\}}}\phi^{(\ell_1+\delta_{1,j})}\wedge\cdots\wedge\phi^{(\ell_n+\delta_{1,j})}=\sum_{\substack{\ell\in\mathscr{L}_i\\ j\in\{1,\cdots,n\}}}\Delta_{\ell+e_j}f\circ\phi=\sum_{\ell\in G(\mathscr{L}_i)}\Delta_\ell f\circ\phi.$$

To conclude, we note that $\Delta_\ell f\circ\phi=0$ whenever ℓ features repeated entries. Hence,

$$\sum_{\ell\in G(\mathscr{L}_i)}\Delta_\ell f\circ\phi=\sum_{\ell\in B\circ G(\mathscr{L}_i)}\Delta_\ell f\circ\phi=\sum_{\ell\in\mathscr{L}_{i+1}}\Delta_\ell f\circ\phi,$$

and we have shown the result. ∎

Proof of Theorem 3.8. Note that we have already proven the $k=1$ case, which we will again use as a base case for induction. Suppose that ϕ is a river of class $k+1$.

For simplicity, introduce the notation $p(t)=\alpha(\dot{\phi}(t),\dots,\phi^{(n)}(t))^{-1}$ so that, by definition,

$$\kappa_\phi(t)=p(t)(\dot{\phi}(t)\wedge\cdots\wedge\phi^{(n)}(t)).$$

Suppose that our assertion is true at the kth level and differentiate to progress to the $(k+1)$ term. Suppressing time dependence,

$$\frac{d^{k+1}}{dt^{k+1}}\kappa_\phi=\sum_{i=0}^{k+1}\binom{k+1}{i}\frac{d^{k+1-i}p}{dt^{k+1-i}}\left(\frac{d^i}{dt^i}\dot{\phi}\wedge\cdots\wedge\phi^{(n)}\right).$$

Application of Lemma 3.9 implies that

$$\sum_{i=0}^{k+1}\binom{k+1}{i}\frac{d^{k+1-i}p}{dt^{k+1-i}}\left(\frac{d^i}{dt^i}\dot{\phi}\wedge\cdots\wedge\phi^{(n)}\right)=\sum_{i=0}^{k+1}\binom{k+1}{i}\frac{d^{k+1-i}p}{dt^{k+1-i}}\sum_{\ell\in\mathscr{L}_i}\Delta_\ell f\circ\phi,$$

which, using our induction hypothesis, simplifies to

$$\frac{d^{k+1}}{dt^{k+1}}\kappa_\phi = p\sum_{\ell\in\mathscr{L}_{k+1}}\Delta_\ell f\circ\phi.$$

Hence, ϕ is a river of class $k+1$ if and only if

$$\sum_{\ell\in\mathscr{L}_i}\Delta_\ell f\circ\phi(0)=0 \qquad \forall i\in\{0,\dots,k+1\},$$

as desired. ∎

With this equivalent condition we can define a confluence of class k.

Definition 3.10. *The set of class k confluences, denoted $C^k_{\mathcal{Z}}$, is given by*

$$C^k_{\mathcal{Z}} = \bigcap_{i=0}^{k}\left\{\sum_{\ell\in\mathscr{L}_i}\Delta_\ell f(x)=0\right\}$$

and a point $x\in\Omega$ is a confluence of class k if $x\in C^k_{\mathcal{Z}}$.

An immediate application of this definition gives the following relationship.

Corollary 3.11. *A trajectory ϕ is a class k river if and only if $\phi(0)$ is a class k confluence.*

In the generic case, the set of class k confluences will be an $n-k-1$ dimensional manifold. Therefore, the strongest river we can expect (generically) in $\mathbb{R}^n$ is of class $n-1$.

4. Normal form results.

4.1. Rivers and canards.

Here we consider the truncated normal form for the flow near a canard point [30],

$$\begin{pmatrix}\dot{x}_1\\ \dot{x}_2\\ \dot{x}_3\end{pmatrix} = \begin{pmatrix}\varepsilon(bx_2+cx_3)\\ \varepsilon a\\ x_1+x_3^2\end{pmatrix} =: f(x;\varepsilon), \tag{4.1}$$

where $0<\varepsilon\ll 1$ is a timescale parameter, $a,b,c\in\mathbb{R}$, and $(0,0,0)$ is the canard point. In system (4.1), we refer to x_1,x_2 as slow variables and x_3 as a fast variable. As a two-timescale system, (4.1) has a critical manifold, given by the set $\mathcal{M}=\{x_1=-x_3^2\}$, where $\dot{x}_3=0$, which can be decomposed into stable and unstable branches and the fold set given by $\mathcal{M}_S=\{x_1=-x_3^2|x_3<0\}, \mathcal{M}_U=\{x_1=-x_3^2|x_3>0\}$, and $\mathcal{M}_F=\{x_1=x_3=0\}$, respectively. Trajectories of interest to us begin near $\mathcal{M}_S$, approach $\mathcal{M}_F$, and linger near $\mathcal{M}_U$ for some amount of time.

To begin our analysis, we will identify the confluences of system (4.1), which we describe in the following proposition.

Proposition 4.1. *If $c^2-8ab>0$ and $b\neq 0$, then there are two branches of infinite-class confluences of system (4.1), given by*

$$C^{\infty}_{\mathcal{Z},\pm} = \left\{ x_1 = -x_3^2 - \frac{\varepsilon}{4}(c \pm \omega), x_2 = -\frac{x_3}{2b}(c \mp \omega) \middle| \, x_3 \in \mathbb{R} \right\},$$

where $\omega := \sqrt{c^2 - 8ab}$. *These branches are invariant in the truncated normal form.*

Proof. Let

$$\Gamma_{\pm}(\eta) = \left(-\eta^2 - \frac{\varepsilon}{4}(c \pm \omega), -\frac{\eta}{2b}(c \mp \omega), \eta \right) \tag{4.2}$$

denote parameterizations of $C^{\infty}_{\mathcal{Z},\pm}$, respectively. First we will demonstrate that the $C^{\infty}_{\mathcal{Z},\pm}$ are invariant under (4.1). If we reparameterize $\Gamma_{\pm}$ by $\Gamma_{\pm} \circ \eta(t)$ for some unknown function η, then

$$\frac{d}{dt}\Gamma_{\pm} \circ \eta(t) = \left(-2\eta, -\frac{c \mp \omega}{2b}, 1 \right) \dot{\eta}$$

and

$$f(\Gamma_{\pm} \circ \eta(t), \varepsilon) = \left(\frac{\varepsilon(c \pm \omega)}{2}\eta, \varepsilon a, -\frac{\epsilon(c \pm \omega)}{4} \right).$$

If we choose

$$\dot{\eta} = -\frac{\varepsilon(c \pm \omega)}{4}, \tag{4.3}$$

then

$$\frac{d}{dt}\Gamma_{\pm} \circ \eta(t) = f(\Gamma_{\pm} \circ \eta(t), \varepsilon)$$

and hence the $C^{\infty}_{\mathcal{Z},\pm}$ are invariant under (4.1). To conclude, we note that $\Gamma_{\pm}$ itself has identically zero curvature, i.e.,

$$\det(\Gamma_{\pm}'(\eta), \Gamma_{\pm}''(\eta), \Gamma_{\pm}'''(\eta)) \equiv 0,$$

which will be preserved under reparameterization. Thus, the trajectories $\phi_{\pm}(t) := \Gamma_{\pm} \circ \eta(t)$ have identically zero curvature for all time, which implies that

$$\kappa_{\phi_{\pm}}(t) = \frac{d}{dt}\kappa_{\phi_{\pm}}(t) = \cdots = \frac{d^k}{dt^k}\kappa_{\phi_{\pm}}(t) = \cdots = 0 \qquad \forall k \in \mathbb{N}, t \in \mathbb{R}, \tag{4.4}$$

and hence the $\Gamma_{\pm}$ parameterize sets of infinite-class confluences. ∎

Corollary 4.2. *If* $c^2 - 8ab > 0$ *and* $b \neq 0$, *then*

$$\phi_{\pm}(t) = \left(-\alpha_{\pm}^2 t^2 - \frac{\varepsilon c}{4} \pm \varepsilon\omega, -\frac{\alpha_{\pm} c t}{2b} \pm \alpha_{\pm}\omega t, \alpha_{\pm} t \right) \tag{4.5}$$

are trajectories of (4.1), *where* $\omega = \sqrt{c^2 - 8ab}, 4\alpha_{\pm} = -\varepsilon(c \pm \omega)$.

Proof. Solving (4.3) with initial condition $\eta(0) = 0$ yields the result. ∎

Corollary 4.3. *The trajectories defined by* (4.5) *are the maximal canards for* $\varepsilon > 0$.

Proof. Note that $\phi_{\pm,1}(t) + \phi_{\pm,3}^2(t) = \mathcal{O}(\varepsilon)$; hence, for all $t \in [0, \infty)$, $\phi_\pm(t)$ is $\mathcal{O}(\varepsilon)$ near the repelling branch of the critical manifold and for all $t \in (-\infty, 0]$, $\phi_\pm(t)$ is $\mathcal{O}(\varepsilon)$ close to the attracting branch of the critical manifold. ∎

Theorem 4.4. *The maximal canards of* (4.1) *are rivers of infinite order.*

Proof. The conditions $c^2 - 8ab > 0, b \neq 0$, are the same conditions presented in [30] for the existence of canards. Specifically, these conditions guarantee that the folded singularity of system (4.1) is not a folded focus or a folded saddle node. The previous proposition with its corollaries demonstrates the result under these conditions. If $c^2 - 8ab \leq 0, b \neq 0$, then the system (4.1) has no maximal canards, and thus the result is vacuously true.

If $b = 0$, then the folded singularity in (4.1) is a folded saddle-node, in which case the base normal form without nonlinear terms becomes [32]

$$\begin{pmatrix} \dot{x}_1 \\ \dot{x}_2 \\ \dot{x}_3 \end{pmatrix} = \begin{pmatrix} \varepsilon\left(\frac{\mu}{2}x_2 - (\mu+1)x_3\right) \\ \varepsilon \\ x_1 + x_3^2 \end{pmatrix}, \tag{4.6}$$

which, following the proof techniques of the previous results, has two invariant branches of infinite-class confluences, given by

$$C^\infty_{\mathcal{Z},j} = \left\{ x_1 = -x_3^2 + \varepsilon\frac{1 + j(\mu-1)}{2}, x_2 = \frac{2x_3}{1 + j(\mu-1)} \middle| x_3 \in \mathbb{R} \right\}$$

for $j \in \{0, 1\}$. Replacing $C^\infty_{\mathcal{Z},\pm}$ with $C^\infty_{\mathcal{Z},j}$ in the previous proofs generates the result. ∎

4.2. Dynamics near the river canard. We will refer to the $C^\infty_{\mathcal{Z},\pm}$ as the *river canard set*. We can use LOR in its simplest form, based on a one-dimensional base curve [20], to understand how trajectories behave near our infinite-class rivers and, in so doing, provide a novel analysis tool for canards.

Specifically, we will perform the LOR transformation based at each of the curves $\Gamma_\pm$ identified in (4.2) in the previous section. Note that, as we demonstrated in the proof of Proposition 4.1, the curves $\Gamma_\pm$ are invariant under the flow of our normal form (4.1) and satisfy (4.4). Therefore we can simplify the LOR equations greatly and the right-hand side of (2.7) becomes [20, 21, 22, 3, 19]:

$$\mathcal{L}_{\Gamma_\pm} f(\eta, \xi) = \begin{pmatrix} \frac{Tf(\eta,\xi)}{\|\Gamma_\pm'(\eta)\|(1-\xi_1\kappa(\eta))} \\ Nf(\eta,\xi) \end{pmatrix}, \tag{4.7}$$

where $\eta \in \mathbb{R}$, $\xi = (\xi_1, \xi_2) \in \mathbb{R}^2$, and $\kappa(\eta)$ is just the usual curvature formula for a curve in three-dimensional space evaluated at $\Gamma_\pm$, which takes the form

$$\kappa_\pm(\eta) = \frac{||\Gamma_\pm'(\eta) \times \Gamma_\pm''(\eta)||}{||\Gamma_\pm'(\eta)||^3} = \frac{||e_\pm'(\eta)||}{||\Gamma_\pm'(\eta)||}$$

for $e_\pm(\eta) = \Gamma_\pm'(\eta)/||\Gamma_\pm'(\eta)||$. The term $Nf(\eta,\xi)$ is the two-dimensional generalization of $g(\eta,\xi)$ from (2.7), corresponding to (2.8) with $k=2$, and takes the form

$$Nf(\eta,\xi) = \begin{pmatrix} \langle f\circ\Psi(\eta,\xi), N_1\Gamma_\pm(\eta)\rangle \\ \langle f\circ\Psi(\eta,\xi), N_2\Gamma_\pm(\eta)\rangle \end{pmatrix},$$

where $\{N_i\Gamma_\pm(\eta) : i=1,2\}$ forms an orthonormal basis for the normal subspace to $\Gamma_\pm$ parameterized by η with (see also [21]) $N_1\Gamma_\pm(\eta)$ the unit normal vector in the direction of $\Gamma_\pm''(\eta) - \langle\Gamma_\pm''(\eta),\Gamma_\pm'(\eta)\rangle\Gamma_\pm'(\eta)/||\Gamma_\pm'(\eta)||^2$.

We will use system (4.7) to understand how trajectories near our river canards are funnelled towards the canard point, linger near the fold, and are pushed away from the repelling manifold $\mathcal{M}_U$; specifically, we will demonstrate that trajectories approach the fold $\mathcal{M}_F$ along one *invariant angular manifold*, experience a short period of unconstrained rotation, and exit the neighborhood of $\mathcal{M}_U$ along another invariant angular manifold. For convenience, we will henceforth drop the $\pm$ subscripts.

To expose the angular dynamics hidden in system (4.7), we will represent the ξ dynamics in polar coordinates. That is, we let $\xi = (r\cos\theta, r\sin\theta)$ and compute the ODEs induced on r,θ, which are given by

$$\begin{aligned} \dot\eta &= \frac{Tf(\eta, r\cos\theta, r\sin\theta)}{\|\Gamma'(\eta)\|(1-r\cos\theta\kappa(\eta))}, \\ \dot r &= \langle(\cos\theta,\sin\theta),\dot\xi\rangle, \\ r\dot\theta &= (\cos\theta,\sin\theta)\wedge\dot\xi. \end{aligned} \tag{4.8}$$

This change of coordinates is functionally equivalent to blowing up the entirety of the river canard trajectory, but we can avoid using the unpleasant chart conventions often associated with this process, as we do not need to increase the dimension of our system.

At first glance, the third equation in (4.8) seems problematic, as we are interested in the region where $r \ll 1$. Note, however, that since $\Gamma_\pm$ are invariant and $\{\xi=0\}$ maps to the set $\{\Gamma_\pm(\eta)|\eta\in\mathbb{R}\}$ under Ψ, we have $Nf(\eta,0)=0$ by Lemma 2.2. Using this observation, we can compute that for any $z(\theta)\in\mathbb{R}^2$,

$$\lim_{r\to0}\frac{z(\theta)\wedge Nf(\eta,rz(\theta))}{r} = \lim_{r\to0}\frac{z(\theta)\wedge D_\xi Nf(\eta,rz(\theta))z(\theta)}{1} = z(\theta)\wedge D_\xi Nf(\eta,0)z(\theta)$$

from L'Hopital's rule. Therefore, the dynamics for small r is given by

$$\begin{aligned} \dot\eta &= \frac{Tf(\eta,0)}{\|\Gamma'(\eta)\|} + \mathcal{O}(r), \\ \dot r &= \langle D_\xi Nf(\eta,0)z(\theta), z(\theta)\rangle r + \mathcal{O}(r^2), \\ \dot\theta &= -D_\xi Nf(\eta,0)z(\theta)\wedge z(\theta) + \mathcal{O}(r), \end{aligned} \tag{4.9}$$

where $z(\theta) = (\cos\theta,\sin\theta)$. In effect, we have performed a geometric desingularization along all of Γ, as the set $\{r=0\}$ is invariant under (4.9). In the process, we have uncovered nontrivial angular dynamics on the set $\{r=0\}$, given by

$$\dot{\eta} = \frac{Tf(\eta,0)}{\|\Gamma'(\eta)\|}, \qquad \dot{\theta} = -D_\xi N f(\eta,0)z(\theta) \wedge z(\theta), \tag{4.10}$$

which will be dominant in the region where $r \ll 1$, in particular near the river canards. Once we understand the dynamics of (4.10), we can piece together a full picture of the dynamics by considering the $\dot{r}$ equation to leading order, to learn how trajectories are drawn to, or pushed away from, the river canards.

First we will study the (η, θ) dynamics in the invariant subset $\{r = 0\}$. Let $A(\eta;\varepsilon) := D_\xi N f(\eta, 0; \varepsilon)$. Using the reparameterization described in (4.3),

$$\frac{Tf(\eta,0)}{\|\Gamma'(\eta)\|} = \frac{-\varepsilon(c \pm \omega)}{4}, \tag{4.11}$$

and therefore system (4.10) is a fast-slow system. Note that this system is invariant under the transformation $\theta \mapsto \theta + \pi$. Hence if $(\eta(t), \theta(t))$ is a solution to (4.10), then $(\eta(t), \theta(t) + \pi)$ will also be a solution. We have a π-shifted family of critical manifold components given by

$$\mathcal{M}_{ang} = \{A(\eta;0)z(\theta) \wedge z(\theta) = 0\},$$

the shape of which will depend on the folded singularity, as illustrated in the examples in Figure 2.

Note that for $x, y \in \mathbb{R}^2$, $x \wedge y = 0$ if and only if $x = cy$ for some scalar c. Hence our critical manifold can be reexpressed as

$$\mathcal{M}_{ang} = \{(\eta,\theta) \,|\, \exists \lambda \text{ such that } A(\eta;0)z(\theta) = \lambda z(\theta)\};$$

that is, $(\eta, \theta) \in \mathcal{M}_{ang}$ if and only if $z(\theta)$ is an eigenvector of $A(\eta; 0)$. Furthermore, as $\|z(\theta)\| = 1$, the eigenvalue associated with $z(\theta)$ must be $\lambda = \langle A(\eta;0)z(\theta), z(\theta)\rangle$. Note that $\langle A(\eta;0)z(\theta), z(\theta)\rangle$ appears as the leading order coeffecient of r in the r equation in (4.9); thus, radial stability is closely related to the angular manifolds. Moreover, using Wolfram Mathematica, we can compute that in the $\varepsilon = 0$ limit, $\det A(\eta;0) = 0$ for all η and therefore the eigenvalues of $A(\eta;0)$ are $0, \mathrm{tr}A(\eta)$. The latter can be computed (also using Wolfram Mathematica) to be 2η from (4.10). We label the corresponding two branches within each component of the critical manifold as

$$\mathcal{M}_{ang,0} = \{(\eta,\theta) \in \mathcal{M}_{ang} | A(\eta;0)z(\theta) = 0\},$$
$$\mathcal{M}_{ang,tr} = \{(\eta,\theta) \in \mathcal{M}_{ang} | A(\eta;0)z(\theta) = 2\eta z(\theta)\}.$$

The stability and hyperbolicity of the critical manifold will be determined by the sign of $\partial\dot{\theta}/\partial\theta$, which can be computed using (4.10):

$$\frac{\partial\dot{\theta}}{\partial\theta} = -A(\eta;0)z'(\theta) \wedge z(\theta) - A(\eta;0)z(\theta) \wedge z'(\theta). \tag{4.12}$$

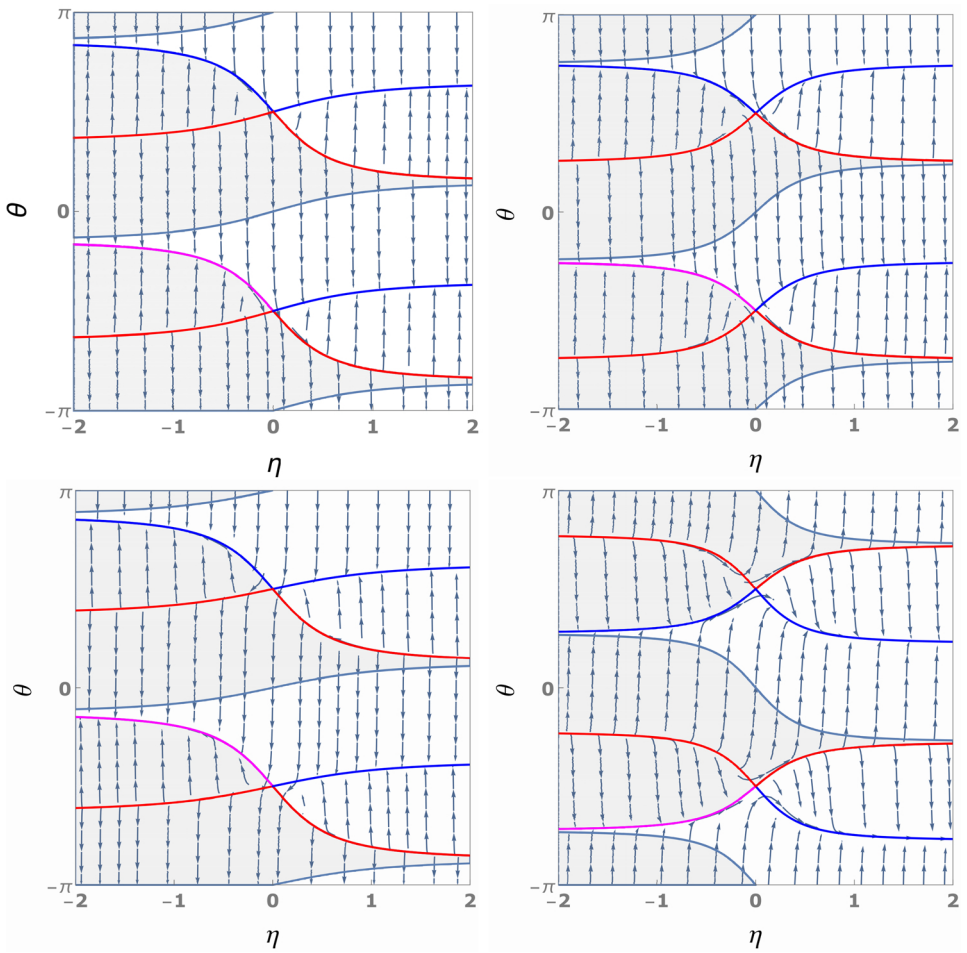

Figure 2. *Four configurations of the angular dynamics. (Upper left) A phase plane plot for system (4.10) derived from the river canard Γ_+ for the folded node ($a = b = 1, c = -3$) case with $\varepsilon = .01$. The colored curves are the slow manifolds of the system; the stable manifolds are shown in blue and purple, and the unstable manifolds are shown in red. The gray region is where $\langle A(\eta;0)z(\theta), z(\theta)\rangle < 0$, which is the region of linear radial stability. (Upper right) The same folded node parameter configuration shown for Γ_-. (Lower left) The angular dynamics of the folded saddle ($-a = b = 2, c = -3$), again with $\varepsilon = .01$, for Γ_+; note that $\dot{\eta} < 0$, hence Γ_+ is a faux canard. (Lower right) The same folded saddle parameter configuration for Γ_-, which is the true canard for the folded saddle system.*

We make use of the following equalities, which hold because $z(\theta)$ is a unit eigenvector such that $z(\theta) \wedge z'(\theta) = 1$,

$$A(\eta;0)z(\theta) \wedge z'(\theta) = \langle A(\eta;0)z(\theta), z(\theta)\rangle,$$
$$-A(\eta;0)z'(\theta) \wedge z(\theta) + A(\eta;0)z(\theta) \wedge z'(\theta) = \mathrm{tr}A(\eta),$$

to express (4.12) as

$$\frac{\partial \dot{\theta}}{\partial \theta} = \mathrm{tr}A(\eta;0) - 2\langle A(\eta;0)z(\theta), z(\theta)\rangle.$$

Given what we have deduced about $\langle A(\eta;0)z(\theta), z(\theta)\rangle$, namely, that it is either 0 or 2η on $\mathcal{M}_{ang}$, and $\mathrm{tr}A(\eta;0) = 2\eta$, we can conclude that

$$\left.\frac{\partial\dot{\theta}}{\partial\theta}\right|_{\mathcal{M}_{ang,0}} = 2\eta, \qquad \left.\frac{\partial\dot{\theta}}{\partial\theta}\right|_{\mathcal{M}_{ang,tr}} = -2\eta$$

and hence the branch of $\mathcal{M}_{ang}$ associated with the zero eigenvalue will be stable for $\eta < 0$, lose hyperbolicity at $\eta = 0$, and become unstable for $\eta > 0$. The branch associated with the other eigenvalue will have the opposite stability.

With this information, we can understand the organization of the $(\eta, \theta, 0)$ plane: trajectories having initial conditions with $\eta < 0$ will be attracted to the set $\{A(\eta;0)z(\theta) = 0\}$ and travel along a branch of this set until $\eta(t) = \mathcal{O}(\varepsilon)$. Trajectories will rotate freely in the neighborhood of $\eta = 0$ until they are drawn to the set $\{A(\eta)z(\theta) = 2\eta z(\theta)\}$ and travel along a corresponding branch of the critical manifold indefinitely. Examples of this behavior appear in Figure 2: trajectories with $\eta < 0$ converge rapidly to an angularly stable purple or blue branch of $\mathcal{M}_{ang,0}$ and drift along it until η nears 0. For such η, trajectories may drift in the direction of decreasing θ to another set of branches of $\mathcal{M}_{ang}$. As η grows away from 0, trajectories settle to a stable blue branch of $\mathcal{M}_{ang}$.

Now we want to add the radial dynamics into the mix. From (4.9), we have

$$\dot{r} = \langle A(\eta;0)z(\theta), z(\theta)\rangle r + h(\eta,\theta)r^2 + \mathcal{O}(\varepsilon),$$

where $h(\eta,\theta)$ is a smooth function that can be computed from (4.7) and turns out to satisfy $h(\eta,\theta+\pi) = -h(\eta,\theta)$. In the domain where r is nonzero but small, we can use our knowledge of the (η,θ) dynamics on $\{r = 0\}$ to approximate the r dynamics.

Suppose that $(\eta(t), r(t), \theta(t))$ is a solution to the system (4.8) with initial condition (η_0, r_0, θ_0). If r_0 is small, then $(\eta(t), \theta(t))$ will be well-approximated by (4.10). Denote by $(\tilde{\eta}(t), \tilde{\theta}(t))$ the solution to (4.10) with initial conditions $(\tilde{\eta}(0), \tilde{\theta}(0)) = (\eta_0, \theta_0)$. To approximate the radial dynamics we will consider the ODE

$$\dot{\tilde{r}} = \langle A(\tilde{\eta};0)z(\tilde{\theta}), z(\tilde{\theta})\rangle\tilde{r} + h(\tilde{\eta},\tilde{\theta})\tilde{r}^2, \tag{4.13}$$

where $\tilde{\eta}, \tilde{\theta}$ are known functions of t. Note from (4.13) that $\tilde{r}$ satisfies a Bernoulli equation, so if $\tilde{r}(0) = r_0$ as well and r_0 is chosen to be small enough, then a Gronwall argument shows that $|r(t) - \tilde{r}(t)|$ will remain $\mathcal{O}(\varepsilon)$ for $\mathcal{O}(1)$ values of t (see [22, Theorem 4.1] for the full details of this argument). Therefore, the condition $\langle A(\tilde{\eta};0)z(\tilde{\theta}), z(\tilde{\theta})\rangle < 0$ largely determines for which $(\tilde{\eta}, \tilde{\theta})$ values trajectories will be attracted towards $\{r = 0\}$; this set is related to the *funnel* in typical canard analysis based on geometric desingularization and is depicted in gray in Figure 2. We have already seen that if $\eta_0 < 0$, then the approximate angular solutions will rapidly approach $\mathcal{M}_{ang,0}$. Our characterization of trajectory behavior is not quite complete, however, because the bilinear form in (4.13) will vanish along $\mathcal{M}_{ang,0}$, since that manifold is defined by $A(\tilde{\eta};0)z(\tilde{\theta}) = 0$. Hence, near each branch of $\mathcal{M}_{ang,0}$, the $\tilde{r}$ dynamics will yield an algebraic decay to or repulsion from $\{\tilde{r} = 0\}$, depending on the quadratic term in (4.13). A calculation shows that this term has opposite signs on each of the π-shifted branches of

$\mathcal{M}_{ang,0}$. We will call these two branches $\mathcal{M}_{ang,0,S}$ and $\mathcal{M}_{ang,0,U}$, respectively, because when it is computed, $h(\eta,\theta)$ turns out to satisfy

$$h(\eta,\theta)\Big|_{\mathcal{M}_{ang,0,S}} < 0 \qquad \text{and} \qquad h(\eta,\theta)\Big|_{\mathcal{M}_{ang,0,U}} > 0. \tag{4.14}$$

This radial effect is not apparent in Figure 2 because the π-shifted branches of $\mathcal{M}_{ang,0}$ appear to have identical relationships with the funnel (for a region of which each forms an upper boundary) and with the angular flow (for which they appear to be stable). Putting everything together, however, we conclude that there is one branch of $\mathcal{M}_{ang,0}$ that will be *radially* stable and *angularly* stable, while the other branch of $\mathcal{M}_{ang,0}$ will be angularly stable and radially unstable. Therefore, the canard solution will only trap trajectories that approach the fold from specific initial angles; this radial and angular analysis together provides the full characterization of the canard funnel effect.

Within the canard funnel, the approximate angular dynamics computed with $r = 0$ predicts that trajectories will approach $\mathcal{M}_{ang,0,S}$ (purple branch in Figure 2). We now see that during at least the final part of this approach, these trajectories will have quadratically decreasing radial components. Therefore, for these solutions, the accuracy of the approximation will increase over time, as $r(t)$ approaches zero. Thus, we can use our approximation up to an $\mathcal{O}(\varepsilon)$ neighborhood of the fold $\{\eta = 0\}$, where the normal hyperbolicity of $\mathcal{M}_{ang,0,S}$ breaks down. The angular manifolds that organize the phase space of system (4.9) for small r are plotted in Figure 3. The figure also shows how these manifolds align in the original LOR frame, with coordinates (η,ξ_1,ξ_2), with and without representation of the blowup of the river into a cylinder. Our analysis shows that in (η,ξ_1,ξ_2) coordinates, trajectories with $\eta < 0$ are pushed away from the red manifold towards the purple and blue manifold. Trajectories may decay radially as they approach the purple and blue branches, but once they approach close enough to the blue branch, they will be repelled from the river, whereas along the purple branch, they will approach the river and the fold of the critical manifold at $\{\eta = 0\}$. In brief, those trajectories that converge towards the fold of the critical manifold contract along the purple branch of the angular invariant manifold as they do so. Finally, the alignment of these structures relative to the original slow manifold after transformation back to the original (x_1,x_2,x_3) coordinates of system (4.1) is illustrated in Figure 4.

To conclude this section, we will study the dynamics of the exit from the vicinity of the slow manifold. To do so, we will show that we can extract the way-in way-out (WIWO) function for the system by using the LOR dynamics. Suppose that $\phi(t) = (\eta(t), r(t), \theta(t))$ is a trajectory with initial conditions $\phi(0) = (\eta_0, r_0, \theta_0)$, which is a point in the funnel (specifically, $\eta_0 < 0$, θ_0 is near $\mathcal{M}_{ang,0,S}$, and $r_0 \ll 1$). ϕ will be drawn towards $r = 0$ until it becomes $\mathcal{O}(\varepsilon)$-close to the fold, $\eta = 0$. As we have previously noted, the radial stability along the angularly stable slow manifold changes as ϕ crosses the fold; beyond the fold, ϕ will be repelled from $r = 0$. However, ϕ will not immediately escape the neighborhood of $r = 0$; indeed, ϕ can be delayed for as long as an $\mathcal{O}(1/\varepsilon)$ time. To explain this delay effect, we will construct the WIWO function.

Define

$$T(r_0,\eta_0) = \inf\{t > 0 | r(t) = r_0, \text{ given that } \eta(0) = \eta_0\},$$

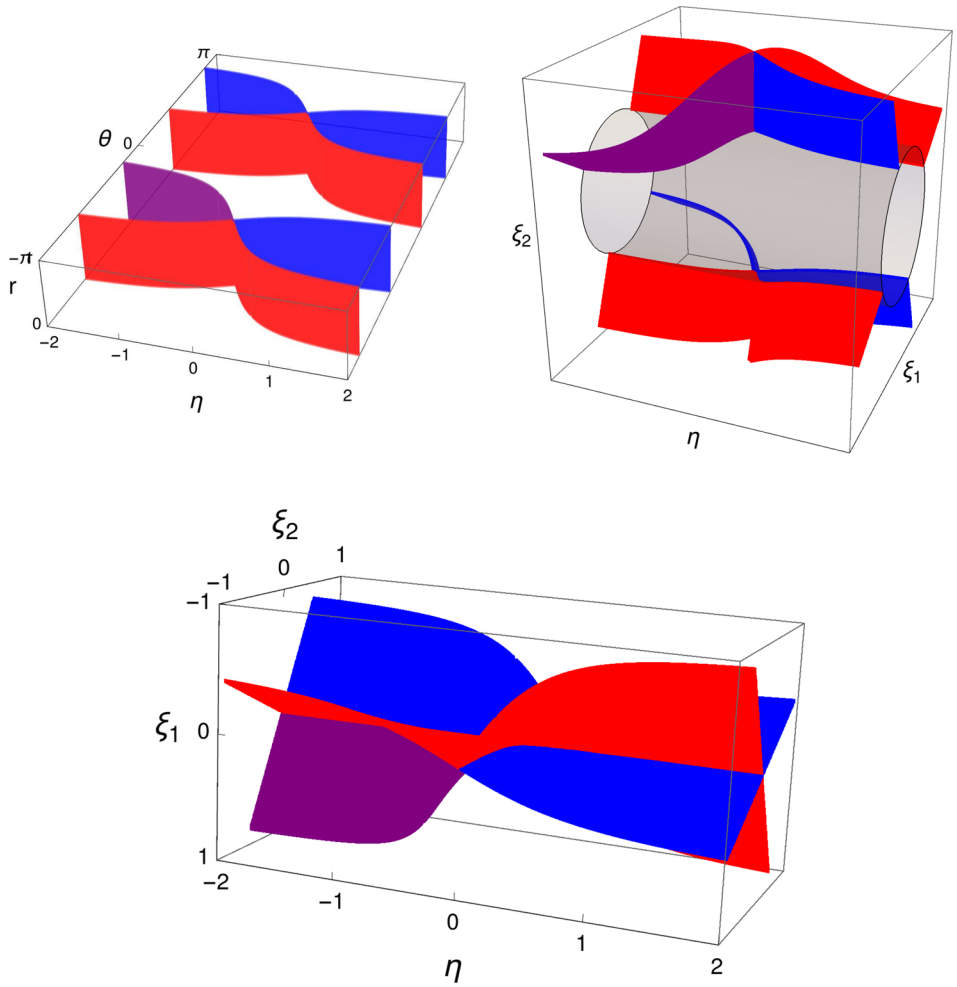

Figure 3. *Angular manifolds that organize passage near the fold. (Upper left) A sketch of the angular manifolds for the* (η, θ, r) *system; for small* r_0*, the* (η, θ) *dynamics will quickly approach their slow limit and be drawn to the angular manifolds that are stable under the angular dynamics. The stable angular manifolds are plotted in blue and purple, and the unstable angular manifolds are shown in red; the purple manifold corresponds to the branch of the stable manifold that is inside the funnel, which is attracting with respect to the* r *dynamics. (Upper right) The angular manfiolds shown in a "blowup" cartoon, in which the manifolds from* the upper left panel *are wrapped around the "cylinder"* $\|\xi\| = 0$*. (Bottom) The angular manifolds in the original LOR coordinates.*

the first positive time for which $r(t)$ returns to its initial value, r_0. As $r(t)$ will decrease until after η has increased through zero, the quantity $T(r_0, \eta_0)$ provides a measure of the time at which $r(t)$ is escaping from zero. The WIWO function is the mapping

$$W(r_0, \eta_0) = \eta \circ T(r_0, \eta_0);$$

that is, W measures the value of η at which r leaves a neighborhood of zero, given that it entered this neighborhood at time $t = 0$ with $\eta = \eta_0$.

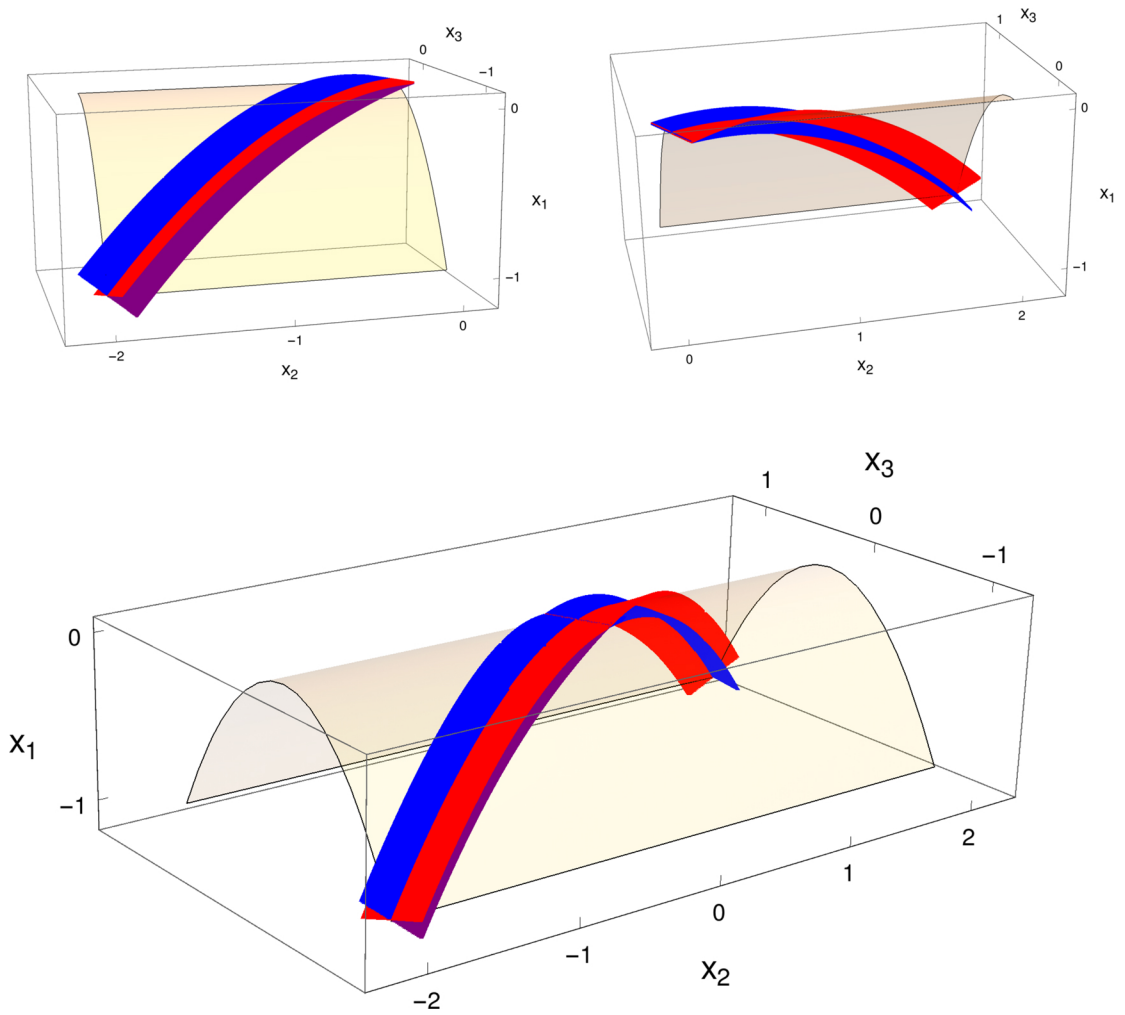

Figure 4. *Organizing angular manifolds in (x_1, x_2, x_3)-space. (Upper left) The angular manifolds mapped back to (x_1, x_2, x_3) space on the attracting ($x_3 < 0$) side of the slow manifold, shown in yellow. Note how the blue and purple stable angular manifolds align with the original slow manifold, while the red unstable angular manifolds, which serve here as funnel separatrices, intersect the original slow manifold tranversely. (Upper right) The exit side of the slow manifold, $x_3 > 0$. Note that here, the unstable angular manifolds in red lie along the original slow manifold, and the blue stable manifolds intersect transversely. (Bottom) The full view of the angular manifolds, combining both the upper left panel and the upper right panel.*

Note that we can numerically integrate the solutions to the full, unapproximated system (4.8) and compute the WIWO function directly, as shown in Figure 5. This is a mechanistically uninformative approach, however, and we can better explain the cause of the delay by approximating the radial dynamics implicitly.

We divide the equations in system (4.10) and apply (4.11) to obtain

$$\frac{d\tilde{\theta}}{d\tilde{\eta}} = \frac{1}{\varepsilon\nu_{\pm}} A(\tilde{\eta}; 0) z(\tilde{\theta}) \wedge z(\tilde{\theta}), \qquad \tilde{\theta}(\eta_0) = \theta_0,$$

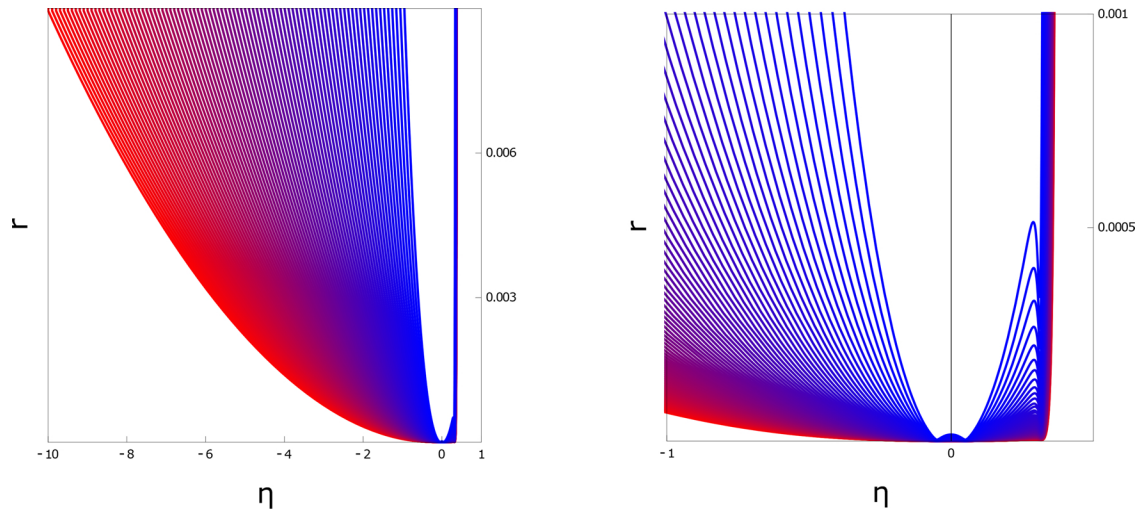

Figure 5. *The radial dynamics near the fold. (Left) Plots of $(\eta(t), r(t))$ for trajectories in the funnel for various η_0 values. All trajectories start at the upper bound of r with η negative. Trajectores plotted in redder colors have more negative η_0 values, while bluer ones have η_0 values closer to zero and hence to the fold. (Right) A zoom near the fold, which displays small radial oscillations in the exiting trajectories.*

where we recall from Corollary 4.2 that $\alpha_\pm = -\varepsilon(c \pm \omega)/4$ comes up in the infinite-class confluences of system (4.1) and we introduce $\nu_\pm = (c \pm \omega)/4$ to keep the ε explicit. From (4.13), an approximation to the r dynamics comes from solving

$$\frac{d\tilde{r}}{d\tilde{\eta}} = -\frac{1}{\varepsilon\nu_\pm}\left(l(\tilde{\eta})\tilde{r} + q(\tilde{\eta})\tilde{r}^2\right), \qquad \tilde{r}(\eta_0) = r_0,$$

where $l(\tilde{\eta}) = \langle A(\tilde{\eta}; 0)z(\tilde{\theta}(\tilde{\eta})), z(\tilde{\theta}(\tilde{\eta}))\rangle, q(\tilde{\eta}) = h(\tilde{\eta}, \tilde{\theta}(\tilde{\eta}))$. This differential equation can be solved explicitly, but we find it most useful to apply the usual transformation $v = 1/\tilde{r}$ for Bernoulli ODEs, multiply the linear ODE in v by an integrating factor, and integrate to transform it to

$$\exp\left(-\frac{1}{\varepsilon\nu_\pm}\int_{\eta_0}^{\tilde{\eta}} l(\sigma)\mathrm{d}\sigma\right)\frac{1}{\tilde{r}(\tilde{\eta})} = \frac{1}{r_0} + \frac{1}{\varepsilon\nu_\pm}\int_{\eta_0}^{\tilde{\eta}} \exp\left(-\frac{1}{\varepsilon\nu_\pm}\int_{\eta_0}^{s} l(\sigma)\mathrm{d}\sigma\right) q(s)\mathrm{d}s.$$

To approximate the $\tilde{\eta} > 0$ at which $\tilde{r}(\tilde{\eta}) = r_0$, we subsititute and rearrange to obtain

$$1 = \exp\left(\frac{L(\tilde{\eta})}{\varepsilon\nu_\pm}\right)\left(1 + \frac{r_0}{\varepsilon\nu_\pm}\int_{\eta_0}^{\tilde{\eta}} \exp\left(-\frac{L(s)}{\varepsilon\nu_\pm}\right) q(s)\mathrm{d}s\right),$$

where $L(\tilde{\eta}) = \int_{\eta_0}^{\tilde{\eta}} l(\sigma)\mathrm{d}\sigma$. Hence

$$-\frac{L(\tilde{\eta})}{\varepsilon\nu_\pm} = \ln\left(1 + \frac{r_0}{\varepsilon\nu_\pm}\int_{\eta_0}^{\tilde{\eta}} \exp\left(-\frac{L(s)}{\varepsilon\nu_\pm}\right) q(s)\mathrm{d}s\right).$$

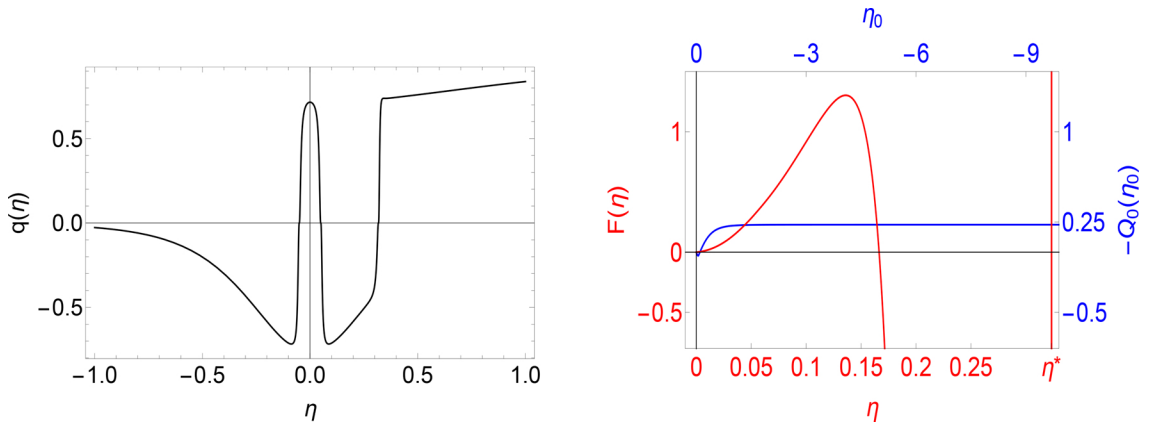

Figure 6. *An approximate WIWO sliderule. In red, we plot the function $F(\eta)$ defined by (4.17) against its independent variable η, the values of which appear on the bottom axis. In blue, we plot $-Q_0(\eta_0)$ against its independent variable η_0, the values of which appear on the top axis. Given an input η_0, to visualize the η value at which escape occurs, we find the η value where $-Q_0(\eta_0)$ is equal to $F(\eta)$. Note that $-Q_0(\eta_0)$ asymptotically approaches $-Q_0^* \approx .23$, and hence this approach estimates that solutions must jump before the final intersection point of the curves, at $\eta* \approx .323$. This matches well with the radial dynamics we observe in Figure 5, where solutions jump near $\eta \approx .33$. Note that the right portion of the red curve is not vertical; however, $F'(\eta^*) \approx 10^{11}$, so F is growing extremely quickly. We use $a = b = 1, c = -3, \varepsilon = 0.01$ for these plots, placing system (4.1) in the folded node regime.*

Since trajectories approach the fold with $\eta < 0$ along $\mathcal{M}_{ang,0}$ where $l(\eta) = 0$ and beyond the fold are attracted to $\mathcal{M}_{ang,tr}$ where $l(\eta) = 2\eta$, it follows that to leading order in ε,

$$L(\eta) = \begin{cases} 0 & \eta < 0, \\ \eta^2 & \eta \geq 0. \end{cases}$$

Making use of $\ln(1+x) = x + \mathcal{O}(x^2)$ we find

$$-\tilde{\eta}^2 = r_0 \left(Q_0(\eta_0) + \int_0^{\tilde{\eta}} \exp\left(\frac{-s^2}{\varepsilon \nu_\pm}\right) q(s) \mathrm{d}s \right) + \mathcal{O}\left(r_0^2\right), \tag{4.15}$$

where $Q_0(\eta_0) = \int_{\eta_0}^0 q(s)\mathrm{d}s$, which we call the quadratic residual. Equation (4.14) gives us $Q_0(\eta_0) < 0$ based on the approximate angular solution, and this inequality will carry over to small nonzero r, which is relevant for $0 < \epsilon \ll 1$, as long as η_0 is not too close to 0. Specifically, Figure 6 shows an example where $q(\eta)$ has its expected negative (positive) sign for $\eta < 0$ ($\eta > 0$) away from 0, but oscillates in the transition between the two.

We rearrange equation (4.15) one more time to obtain the final form

$$\int_0^{\tilde{\eta}} \exp\left(-\frac{s^2}{\varepsilon \nu_\pm}\right) q(s)\mathrm{d}s + \frac{\tilde{\eta}^2}{r_0} = -Q_0(\eta_0) + \mathcal{O}(r_0). \tag{4.16}$$

Equation (4.16) can be solved for $\tilde{\eta}$ to find the approximate η value at which r grows back to r_0. This escape condition shows that in order to escape from the river canard, the trajectory must overcome the quadratic residual term. The integral on the left-hand side of (4.16) will

diverge rapidly from zero, since $\nu_\pm < 0$ (consistent with $\dot{\eta} > 0$). Note, however, that the integral need not grow monotonically immediately beyond $\tilde{\eta} = 0$. Indeed, dropping the tilde for convenience and defining

$$F(\eta) = \int_0^\eta \exp\left(-\frac{s^2}{\varepsilon\nu_\pm}\right) q(s)\mathrm{d}s + \frac{\eta^2}{r_0}, \tag{4.17}$$

we find that $F(\eta)$ first increases and then decreases before increasing again, consistent with the behavior of $q(\eta)$ and the positive contribution of η^2/r_0 (Figure 6).

Note that the left-hand side of the escape condition (4.16) is approach-agnostic; changing η_0 will only affect $Q_0(\eta_0)$ on the right-hand side. One of the more curious features of the delayed escape from a canard point is the buffer point effect: a buffer point is a value η^* such that all trajectories will leave the river canard before $\eta = \eta^*$, regardless of η_0. In some sense, the buffer point is the longest a solution can be delayed. In our LOR system, the buffer point phenomenon is easily understood; sending $\eta_0 \to -\infty$, we find

$$\lim_{\eta_0 \to -\infty} Q_0(\eta_0) = Q_0^*,$$

i.e., $q(s)$ is integrable on $(-\infty, 0]$, and hence our quadratic residual will always have finite size. The rapidly diverging integral will always overcome Q_0^*, hence the buffer point solves $F(\eta^*) = -Q_0^*$. Empirically, we see that based on the asymptotic behavior of $-Q_0(\eta_0)$ and the eventual rapid growth of $F(\eta)$, (4.16) does an excellent job approximating the buffer point η^* by which all orbits jump away; however, the terms that we have neglected can introduce spurious solutions for smaller η (Figure 6).

The preceding analysis is summarized in the following proposition.

Proposition 4.5. *The WIWO function, $W(\eta_0, r_0)$, satisfies*

$$-\frac{L \circ W(\eta_0, r_0)}{\varepsilon\nu_\pm} = \ln\left(1 + \frac{r_0}{\varepsilon\nu_\pm}\int_{\eta_0}^{W(\eta_0,r_0)} \exp\left(-\frac{L(s)}{\varepsilon\nu_\pm}\right) q(s)\mathrm{d}s\right)$$

and can be approximated for small r_0, ε by the solution to

$$F \circ W(\eta_0, r_0) = -Q_0(\eta_0) + \mathcal{O}(r_0),$$

where

$$F(\eta) = \int_0^\eta \exp\left(-\frac{s^2}{\varepsilon\nu_\pm}\right) q(s)\mathrm{d}s + \frac{\eta^2}{r_0}$$

and

$$Q_0(\eta_0) = \int_{\eta_0}^0 q(s)\mathrm{d}s.$$

For

$$Q_0^* := \lim_{\eta_0 \to -\infty} Q_0(\eta_0),$$

all trajectories in the funnel must exit a tube of radius r_0 around $\Gamma_\pm$ before η reaches the value η^* given up to $\mathcal{O}(r_0)$ by

$$F(\eta^*) = -Q_0^*.$$

The LOR frame has given us a new perspective on the dynamics near our river canard solutions. Instead of tracking solutions through multiple blowup charts, we can desingularize the dynamics along the entire river canard trajectory. By approximating the radial dynamics explicitly, we can estimate passage time along the fold using a WIWO function conveniently expressed in terms of a timelike variable η. Moreover, although previous analysis had derived a WIWO function, also given as an upper limit of an integral, which can be used to compute a passage time and to prove the existence of the buffer point, that result did not include the decomposition into geometric components that we provide and its derivation used complexification of time to evaluate WIWO integrals along elliptical contours [18], which we avoid here. Our approach also highlights the essential asymmetry in the way that nearby trajectories approach and depart from the neighborhood of the fold; trajectories in the funnel region, which itself is the product of quadratic stability, will be drawn to $r = 0$ algebraically yet will escape exponentially. Overall, by viewing the normal form flow from the perspective of the river canards, we expose nontrivial dynamics in a geometric way.

5. Transformations.

In the previous section, we established that for the leading order part of the normal form for the flow near a canard point, system (4.1), the maximal canards are rivers of infinite order, and nearby trajectories approach and depart the fold along stable invariant angular manifolds that we have identified, after spending a time period near the fold that we can bound using a WIWO function. Here, we consider how these results generalize beyond the truncated normal form in three-dimensional systems ($n = 3$).

5.1. Nearly curvature preserving maps.

In this section we consider systems with 1 fast and 2 slow variables, or 1-fast 2-slow systems, in $\mathbb{R}^3$. First we will establish two computational lemmas. The crux of these results is understanding how certain transformations of a flow affect the curvature of the flow. Recall that the function Δ_l was defined in (3.1) and the set $\mathscr{L}$ was defined in Definition 3.7.

Definition 5.1. *Suppose that $\dot{x} = f(x)$ induces a flow for $x \in \mathbb{R}^3$, and $H : \mathbb{R}^3 \to \mathbb{R}^3$ is a smooth diffeomorphism. For $y = H(x)$, the flow*

$$\dot{y} = [D_x H(x)]\dot{x} = [D_x H \circ H^{-1}(y)]f \circ H^{-1}(y) =: g(y)$$

is induced on y. If $\Delta_\ell f(x) = 0$, then we say that H is Δ_ℓ-preserving if $\Delta_\ell(g \circ H(x)) = 0$ for all $\ell \in \mathscr{L}$.

If $\dot{x} = f(x)$ is a fast-slow system with timescale parameter $0 < \varepsilon \ll 1$ and $\Delta_\ell f(x) = 0$, then we say that H is nearly Δ_ℓ-preserving to order k if there exists a smooth, positive definite, $\mathcal{O}(1)$ map $C(x)$ such that

$$C(x)\Delta_\ell f(x) - \Delta_\ell(g \circ H(x)) = \mathcal{O}(\varepsilon^k) \tag{5.1}$$

uniformly for all x in an $\mathcal{O}(\varepsilon)$ neighborhood of the critical manifold.

We can also define H as locally nearly Δ_ℓ-preserving to order k if (5.1) holds on a compact submanifold of the critical manifold; the local property will suffice for our purposes, but we will drop the word "locally" in the text below. Note that, since curvature is a geometric property, most nonlinear maps are not nearly Δ_ℓ-preserving.

Lemma 5.2. *Nondegenerate linear mappings are Δ_l-preserving for all l.*

Proof. In the case $H(x) = Ax$, where A is invertible, it is simple to compute $y^{(i)} = Ax^{(i)}$ so $\Delta_\ell(g \circ H(x)) = \det(A)\Delta_\ell f(x)$. ∎

Lemma 5.3. *Given a 1-fast 2-slow system*

$$\dot{x} = \begin{pmatrix} \varepsilon g_1(x_1, x_2, x_3; \varepsilon) \\ \varepsilon g_2(x_1, x_2, x_3; \varepsilon) \\ F(x_1, x_2, x_3; \varepsilon) \end{pmatrix} =: f(x; \varepsilon) \tag{5.2}$$

with $\Delta_\ell f(x) = 0$, all near-identity transformations $H(x; \varepsilon)$ are nearly Δ_ℓ-preserving to order $|\ell| + 1$.

Proof. Given a near-identity transformation $H(x; \varepsilon)$, we can write $H(x; \varepsilon) = x + \varepsilon h(x; \varepsilon)$ and inductively compute that when x is in an $\mathcal{O}(\varepsilon)$ neighborhood of the critical manifold,

$$y^{(i)} = (I + \varepsilon D_x h(x, \varepsilon))\, x^{(i)} + \mathcal{O}(\varepsilon^{i+1}),$$

where I is the identity matrix. Here we have used the fact that, when x is $\mathcal{O}(\varepsilon)$ close to the critical manifold, $x^{(i)} = \mathcal{O}(\varepsilon^i)$. Computing the wedge products

$$\Delta_\ell(g \circ H(x)) = \det(I + \varepsilon D_x h(x; \varepsilon))\Delta_\ell f(x) + \mathcal{O}\left(\varepsilon^{|\ell|+1}\right)$$

and taking $C(x) = \det(I + \varepsilon D_x h(x; \varepsilon)) = 1 + \mathcal{O}(\varepsilon)$ proves the result. ∎

Note that in a fast-slow system, when x is $\mathcal{O}(\varepsilon)$ close to the critical manifold, direct computation shows that $\Delta_\ell f(x; \varepsilon) = \mathcal{O}(\varepsilon^{|\ell|})$, such that it has the form

$$\Delta_\ell f(x; \varepsilon) = \frac{\partial^{|\ell|}}{\partial \varepsilon^{|\ell|}} \Delta_\ell f(x; 0) \frac{\varepsilon^{|\ell|}}{|\ell|!} + \mathcal{O}\left(\varepsilon^{|\ell|+1}\right)$$

from Taylor's equation.

Definition 5.4. *Let $B(\mathcal{M}, \mathcal{O}(\varepsilon))$ denote a ball with $\mathcal{O}(\varepsilon)$ radius around the manifold $\mathcal{M}$. The set of class k near-confluences, denoted by $C^k_{\mathcal{Z},\varepsilon}$, is given by*

$$C^k_{\mathcal{Z},\varepsilon} = \bigcap_{i=0}^{k} \left\{ x \in B(\mathcal{M}, \mathcal{O}(\varepsilon)) \,\middle|\, \sum_{\ell \in \mathscr{L}_i} \frac{\partial^{|\ell|}}{\partial \varepsilon^{|\ell|}} \Delta_\ell f(x; 0) = 0 \right\}.$$

A class k weak river is a trajectory ϕ such that $\phi(0)$ is a class k near-confluence.

5.2. On the nonexistence of terrestrial canards. Combining Definition 5.4 with Lemmas 5.2, 5.3 and Theorem 4.4 yields the following result.

Theorem 5.5. *Given a* 1*-fast* 2*-slow system of the form* (5.2) *that features a canard point, the canard solutions to* (5.2) *lie* $\mathcal{O}(\varepsilon)$ *close to the set* $C^3_{\mathcal{Z},\varepsilon}$.

Proof. Since (5.2) features a canard point, there are a sequence of linear and near-identity transformations that convert (5.2) to the canard point normal form. We have already demonstrated the existence of river canard solutions to the truncated normal form, system (4.1), in Theorem 4.4. Applying the inverse linear and near-identity transformations (which are themselves linear and near-identity transformations, respectively), we can track the set $C^3_{\mathcal{Z}}$ using Lemmas 5.2 and 5.3; namely, it will be mapped to the set $C^3_{\mathcal{Z},\varepsilon}$. Finally, we note that under the inverse linear and near-identity transformations the canard solution of the normal form (4.1) must remain $\mathcal{O}(\varepsilon)$ close to the image of $C^3_{\mathcal{Z}}$. ∎

As the set $C^3_{\mathcal{Z},\varepsilon}$ can be computed with the aid of numerical or symbolic computational tools, we can use $C^3_{\mathcal{Z},\varepsilon}$ to find the canard solutions of any 1-fast, 2-slow system in which they exist. More details on the exact nature of this computation are given for a specific example system in the following section; however, the outline of the process is quite simple: given the system (5.2) we identify $C^3_{\mathcal{Z},\varepsilon}$ by computing series expansions of $\Delta_{1,2,3}, \Delta_{1,2,4}$, and $\Delta_{1,2,5} + \Delta_{1,3,4}$ in ε, and then we use $C^3_{\mathcal{Z},\varepsilon}$ as a pool of initial conditions. The trajectories through $C^3_{\mathcal{Z},\varepsilon}$ will be $\mathcal{O}(\varepsilon)$ close to the canard solution we desire. Indeed, all canards must stay $\mathcal{O}(\varepsilon)$ close to weak rivers. In brief, *all ducks live in rivers*, at least in 1-fast, 2-slow systems.

6. The autocatalator system.

In this section, we present a well-known example of a system that displays canard solutions, the autocatalator system. Specifically, we will study the dynamics given by

$$\begin{aligned} \dot{a} &= \varepsilon\left(\mu\left(\frac{5}{2}+c\right) - ab^2 - a\right), \\ \dot{b} &= ab^2 + a - b, \\ \dot{c} &= \varepsilon(b-c), \end{aligned} \tag{6.1}$$

where $0 < \varepsilon \ll 1, \mu > 0$ are parameters. The system represents the dynamics of a chemical reaction involving three reactants, the concentrations of which are proportional to a, b, c, respectively. In this reaction schema, reactant B slowly bolsters the concentration of reactant C, which in turn boosts production of reactant A. Meanwhile, A and B react to produce more of B but also to inhibit the production of A. In brief, through C, B promotes the buildup of A, with which it reacts to form more B, giving rise to the name of the system. Because of the physical interpretations of the variables, we focus on the positively invariant positive orthant of the system.

In the singular limit, we find $\mathcal{M} = \{a = b/(1+b^2)\}$ to be the critical manifold of the system, with stable branch, unstable branch, and fold given by

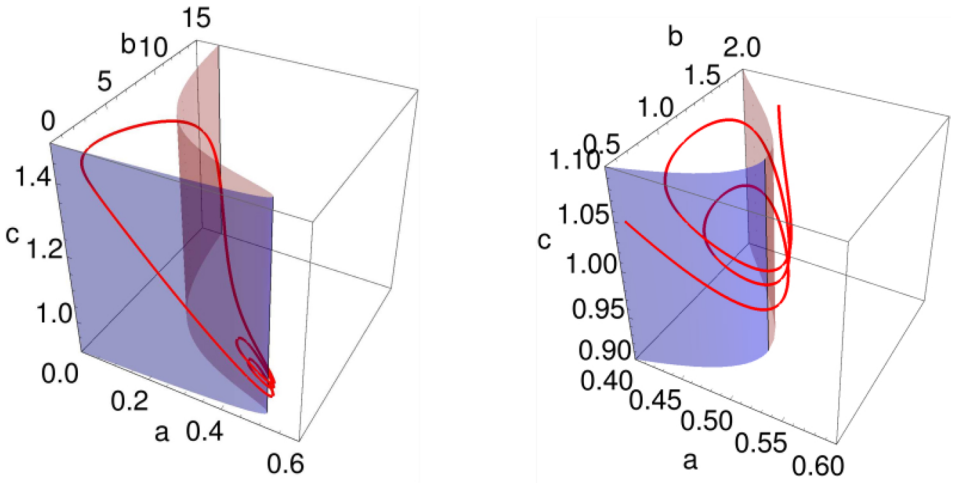

Figure 7. *The attractor of the autocalator system (6.1). (Left) The red trajectory is the attractor for $\varepsilon = 0.013, \mu = 0.299$. The stable branch of the critical manifold, $\mathcal{M}_S$, is shown in light blue, and the unstable branch of the critical manifold, $\mathcal{M}_U$, is shown in light red. (Right) A zoom on the attractor near the canard point $(1/2, 1, 1)$. Note from the two panels together that the attractor exhibits multiscale oscillations.*

$$\mathcal{M}_S = \left\{ a = \frac{b}{1+b^2}, b < 1 \right\},$$
$$\mathcal{M}_U = \left\{ a = \frac{b}{1+b^2}, b > 1 \right\},$$
$$\mathcal{M}_F = \left\{ a = \frac{b}{1+b^2}, b = 1 \right\},$$

respectively.

It is known that system (6.1) has a canard point at $a = 1/2, b = 1, c = 1$ [24]. Indeed, the canard trajectories of the system contribute to the form of the attractor of the system, which is a mixed-mode oscillation (Figure 7). Note that (6.1) exhibits a large-scale oscillation that is modulated by smaller amplitude oscillations.

We will verify that the canard solutions of (6.1) lie near weak rivers. Recall that weak rivers must lie $\mathcal{O}(\varepsilon)$ close to the critical manifold. Thus, we numerically search for near-confluences in a tube around the manfiold; that is, we minimize $|\Delta_{1,2,3}f|, |\Delta_{1,2,4}f|, |\Delta_{1,2,5}f + \Delta_{1,3,4}f|$ on the set $B(\mathcal{M}, \varepsilon)$. Interestingly, we find an actual confluence point (i.e., $\Delta_{1,2,3}f = 0, \Delta_{1,2,4}f = 0, \Delta_{1,2,5}f + \Delta_{1,3,4}f = 0$) at $(a, b, c) \approx (0.499, 1.066, 1.066)$, which is not guaranteed by our theory, but is a nice proof of concept.

Using a symbolic computation engine (Wolfram Mathematica) we find a set of class 2 near-confluences (i.e., elements of $C^2_{\mathcal{Z},\varepsilon}$) near the fold (Figure 8). To find the weak river, we minimize $|\Delta_{1,2,5}f + \Delta_{1,3,4}f|$ along the relevant branch of $C^2_{\mathcal{Z},\varepsilon}$; in fact, we find that the minimum occurs at $(a^*, b^*, c^*) \approx (0.495, 1.07, 1.04)$, very close to the previously mentioned confluence point and the canard point. We find that $|\Delta_{1,2,5}f(a^*, b^*, c^*) + \Delta_{1,3,4}f(a^*, b^*, c^*)| \approx \varepsilon^{7.42}$, which places it reasonably close to the desired $\varepsilon^{|\ell|}$, based on Lemma 5.3, since here $|\ell| = 8$.

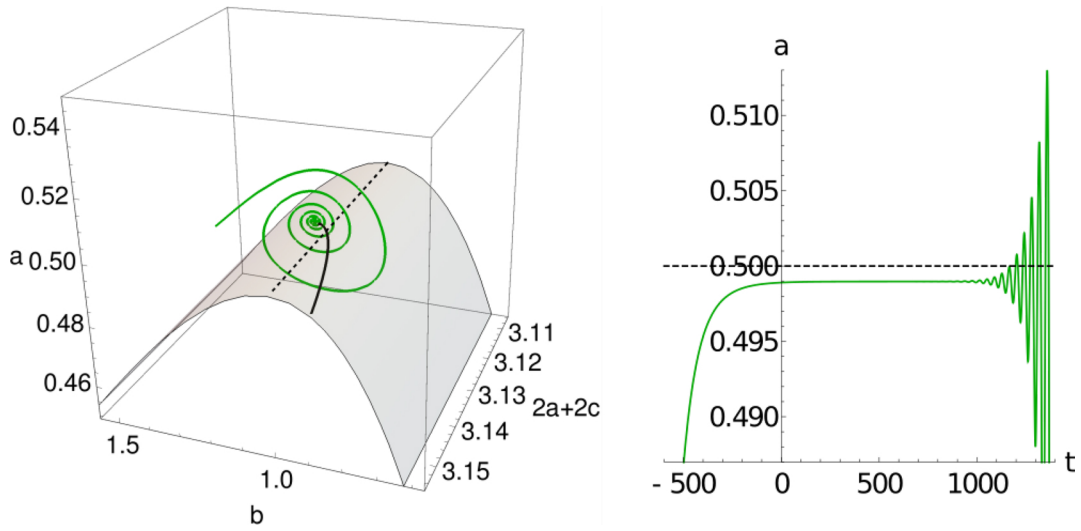

Figure 8. *The near-confluences $C^2_{\mathcal{Z},\varepsilon}$ leading to the canard point. (Left) The near-confluence set $C^2_{\mathcal{Z},\varepsilon}$ (black) lies near the critical manifold (gray) and passes near the fold (dashed black). The green curve is the trajectory, or weak river, through the point on $C^2_{\mathcal{Z},\varepsilon}$ that has minimal $|\Delta_{1,2,5}f + \Delta_{1,3,4}f|$; the canard solutions near the fold lie $O(\varepsilon)$ close to this curve. Note that the axes here are $a, b, 2a + 2c$, which provide a clearer visualization than a, b, c. (Right) Along the weak river, a long delay occurs near $a = 1/2$ and is followed by the onset of gradually growing, small amplitude oscillations.*

Denote by $\phi(t)$ the trajectory through our minimum (a^*, b^*, c^*), which is the desired weak river. We claim that this trajectory has all of the hallmark characteristics of a canard solution. The right portion of Figure 8 shows that ϕ lingers near the canard point for an $\mathcal{O}(1/\varepsilon)$ amount of time, and upon its exit from the canard point it exhibits small scale oscillations that rapidly grow.

To conclude this section, we demonstrate how we can use the near-confluence set $C^2_{\mathcal{Z},\varepsilon}$ to approximate the perturbed slow manifold. It is well known that the perturbed slow manifolds near a canard point will exhibit a complicated twisted shape due to the rotational influence of the canard solution [30, 32]. To approximate these twisting manifolds, we flow the points of $C^2_{\mathcal{Z},\varepsilon}$ forward in time; as canard solutions must lie $\mathcal{O}(\epsilon)$ close to $C^3_{\mathcal{Z},\varepsilon} \subset C^2_{\mathcal{Z},\varepsilon}$ by Theorem 5.5 and also must lie on $\mathcal{M}_{S,\varepsilon}$, the trajectories that flow from $C^2_{\mathcal{Z},\varepsilon}$ will be a good approximation of $\mathcal{M}_{S,\varepsilon}$. Two views of this continuum of trajectories are shown in Figure 9.

In the standard numerical approach, one starts by numerically approximating the perturbed slow manifolds $\mathcal{M}_{S,\varepsilon}, \mathcal{M}_{U,\varepsilon}$, usually using a boundary value problem formulation [32]. The canard solution is subsequently found by computing the intersection $\mathcal{M}_{S,\varepsilon} \cap \mathcal{M}_{U,\varepsilon}$, as the canard solution begins on $\mathcal{M}_{S,\varepsilon}$ and crosses into $\mathcal{M}_{U,\varepsilon}$ [30, 32]. In our formulation of this computation, we reverse the order: we first identify the canard solution and use the results of that computation to identify the perturbed slow manifold. There is no obvious way to identify secondary canards using curvature methods, however.

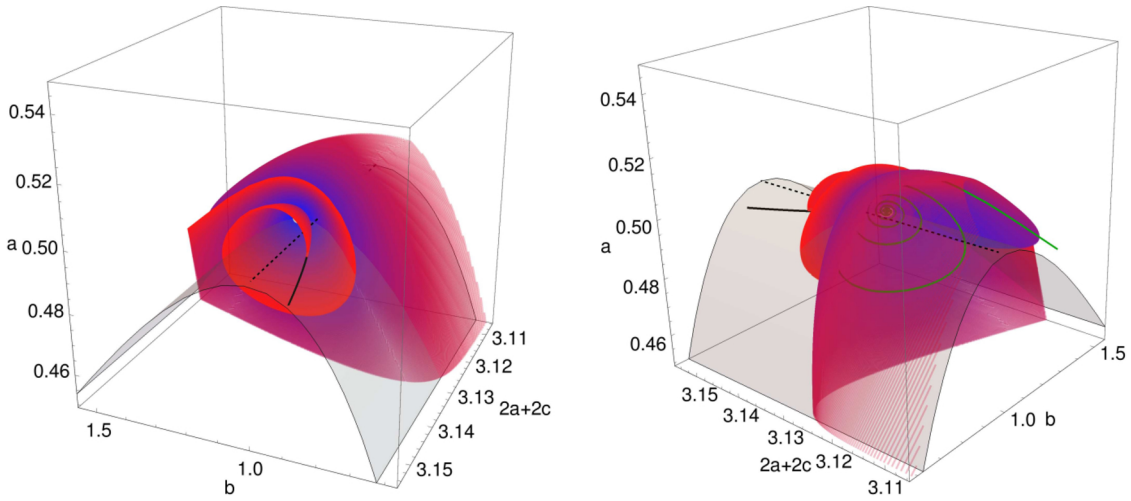

Figure 9. *Approximation of $\mathcal{M}_{S,\varepsilon}$ for system (6.1) viewed from two different angles. We overlay the trajectories with initial conditions in $C^2_{\mathcal{Z},\varepsilon}$ near the fold (dashed black) of the critical manifold (gray). Trajectories with initial conditions farther from the fold are colored in red, while trajectories with initial conditions nearer to the fold are colored bluer. The set $C^2_{\mathcal{Z},\varepsilon}$ is shown in solid black and the canard solution (only visible in the right panel) in green. Note that we again plot $2a + 2c$ in place of c.*

7. Conclusion. Past work has established the existence of a funnel, through which trajectories are squeezed as they approach a canard point [12, 33, 8, 18]. We have recently shown that contraction of trajectories can be associated with special solutions called rivers, emanating from confluence points [20]. In this work, we connect these two concepts, generalizing rivers to arbitrary dimensions and showing that, at least in 1-fast, 2-slow systems, all canards must lie near a form of river. We have provided formulas that define these rivers and can be used to locate them computationally. Moreover, our findings include additional new results: the funnel can be represented as an invariant manifold of a transformed system, the LOR equations, and computed numerically using a blowup along the river, while the duration of the prolonged time of passage near the fold that trajectories experience can be closely approximated using the same blownup system, without a transformation to complex time [18], which should significantly facilitate calculations for model systems in applications. The WIWO functions used to compute passage times (e.g., [5, 32, 15]) are also applied to calculate delays in escape after slow passage through a subcritical fast subsystem Hopf bifurcation on a critical manifold in systems with $m \geq 2$ fast variables and $k \geq 1$ slow variables [25, 26, 18]. Although canards are not present in standard delayed Hopf bifurcations, when $k = 1$, the critical manifold itself is trivially a river. Hence, developing a WIWO calculation based on the blowup ideas in section 4.2 of this paper would be an interesting direction for future research.

This work represents an application of LOR. LOR is a powerful geometric technique for transforming vector fields into coordinate systems highlighting tangential and orthogonal dynamics (see also [36, 4, 23, 29, 38] for related ideas) relative to any curve or surface in the phase space. In past work, we have used LOR to define, locate, and study the influence of rivers in the plane [20] as well as to locate periodic orbits and analyze orbit stability and

the dynamics of trajectories as they approach stable periodics [22]. LOR can be applied in arbitrary dimensions [21], but the results relating canards and rivers in this paper are restricted to 1-fast, 2-slow systems in $\mathbb{R}^3$. This is a central setting in which to work, since 1-fast and 2-slow variables have been shown to underlie robust canard dynamics, even when they arise in higher-dimensional systems [34]. Nonetheless, it would be interesting to work out the details of the precise relation of canards and rivers in higher dimensions, which currently remains an open problem.

REFERENCES

[1] R. Bertam and J. E. Rubin, *Multi-timescale systems and fast-slow analysis*, Math. Biosci., 287 (2017), pp. 105–121.

[2] C. Börgers and N. Kopell, *Synchronization in networks of excitatory and inhibitory neurons with sparse, random connectivity*, Neural Comput., 15 (2003), pp. 509–538.

[3] J. W. Bruce and P. J. Giblin, *Curves and Singularities: A Geometrical Introduction to Singularity Theory*, Cambridge University Press, Cambridge, 1992.

[4] O. Castejón, A. Guillamon, and G. Huguet, *Phase-amplitude response functions for transient-state stimuli*, J. Math. Neurosci., 3 (2013), 13.

[5] R. Curtu and J. Rubin, *Interaction of canard and singular Hopf mechanisms in a neural model*, SIAM J. Appl. Dyn. Syst., 10 (2011), pp. 1443–1479.

[6] J. Day, J. Rubin, Y. Vodovotz, C. C. Chow, A. Reynolds, and G. Clermont, *A reduced mathematical model of the acute inflammatory response* II. *Capturing scenarios of repeated endotoxin administration*, J. Theoret. Biol., 242 (2006), pp. 237–256.

[7] M. Desroches, J. Guckenheimer, B. Krauskopf, C. Kuehn, H. M. Osinga, and M. Wechselberger, *Mixed-mode oscillations with multiple time scales*, SIAM Rev., 54 (2012), pp. 211–288.

[8] M. Desroches, B. Krauskopf, and H. M. Osinga, *The geometry of slow manifolds near a folded node*, SIAM J. Appl. Dyn. Syst., 7 (2008), pp. 1131–1162.

[9] F. Diener, *Proprietes asymptotiques des fleuves*, C. R. Acad. Sci. Paris, 302 (1986), pp. 55–58.

[10] M. Diener, *Determination et existence des fleuves en dimension deux*, C. R. Acad. Sci. Paris, 301 (1985), pp. 899–914.

[11] N. Fenichel, *Geometric singular perturbation theory for ordinary differential equations*, J. Differential Equations, 31 (1979), pp. 53–98.

[12] J. Guckenheimer and R. Haiduc, *Canards at folded nodes*, Mosc. Math. J., 5 (2005), pp. 91–103.

[13] G. Haller, *Lagrangian coherent structures*, Annu. Rev. Fluid Mech., 47 (2015), pp. 137–162.

[14] A. Hastings, K. C. Abbott, K. Cuddington, T. Francis, G. Gellner, Y.-C. Lai, A. Morozov, S. Petrovskii, K. Scranton, and M. L. Zeeman, *Transient phenomena in ecology*, Science, 361 (2018), eaat6412.

[15] M. G. Hayes, T. J. Kaper, P. Szmolyan, and M. Wechselberger, *Geometric desingularization of degenerate singularities in the presence of fast rotation: A new proof of known results for slow passage through Hopf bifurcations*, Indag. Math. (N.S.), 27 (2016), pp. 1184–1203.

[16] C. K. R. T. Jones, *Geometric Singular Perturbation Theory*, in Dynamical Systems, Lecture Notes in Math. 1609, Springer, Berlin, 1995, pp. 44–120.

[17] M. Krupa and P. Szmolyan, *Extending geometric singular perturbation theory to nonhyperbolic points—fold and canard points in two dimensions*, SIAM J. Math. Anal., 33 (2001), pp. 286–314.

[18] M. Krupa and M. Wechselberger, *Local analysis near a folded saddle-node singularity*, J. Differential Equations, 248 (2010), pp. 2841–2888.

[19] W. Kühnel, *Differential Geometry: Curves-Surfaces-Manifolds*, Stud. Math. Libr. 16, 2nd ed., American Mathematical Society, Providence, RI, 2006.

[20] B. Letson and J. E. Rubin, *A new frame for an old (phase) portrait: Finding rivers and other flow features in the plane*, SIAM J. Appl. Dyn. Syst., 17 (2018), pp. 2414–2445.

[21] B. Letson and J. E. Rubin, *Local orthogonal rectification: Deriving natural coordinates to study flows relative to manifolds*, Discrete Contin. Dyn. Syst. Ser. B, 25 (2020), 3725.

[22] B. Letson and J. E. Rubin, *LOR for analysis of periodic dynamics: A one-stop shop approach*, SIAM J. Appl. Dyn. Syst., 19 (2020), pp. 58–84.
[23] A. Mauroy, I. Mezic, and J. Moehlis, *Isostables, isochrons, and Koopman spectrum for the action-angle representation of stable fixed point dynamics*, Phys. D, 261 (2013), pp. 19–30.
[24] A. Milik, P. Szmolyan, H. Löffelmann, and E. Gröller, *Geometry of mixed-mode oscillations in the* 3*-d autocatalator*, Internat. J. Bifur. Chaos, 8 (1998), pp. 505–519.
[25] A. Neishtadt, *Persistence of stability loss for dynamical bifurcations.* I., Differ. Uravn., 23 (1987), pp. 2060–2067 (in Russian); Differ. Equ., 23 (1988), pp. 1385−1391 (in English).
[26] A. Neishtadt, *Persistence of stability loss for dynamical bifurcations.* II., Differ. Uravn., 24 (1988), pp. 226–233.
[27] M. Rabinovich, R. Huerta, and G. Laurent, *Transient dynamics for neural processing*, Science, 321 (2008), pp. 48–50.
[28] J. Rubin and M. Wechselberger, *Giant squid-hidden canard: The* 3*d geometry of the Hodgkin-Huxley model*, Biol. Cybernet., 97 (2007), pp. 5–32.
[29] S. Shirasaka, W. Kurebayashi, and H. Nakao, *Phase-amplitude reduction of transient dynamics far from attractors for limit-cycling systems*, Chaos, 27 (2017), 023119.
[30] P. Szmolyan and M. Wechselberger, *Canards in* $\mathbb{R}^3$, J. Differential Equations, 177 (2001), pp. 419–453.
[31] D. Terman, J. E. Rubin, and C. O. Diekman, *Irregular activity arises as a natural consequence of synaptic inhibition*, Chaos, 23 (2013), 046110.
[32] T. Vo and M. Wechselberger, *Canards of folded saddle-node type* I, SIAM J. Math. Anal., 47 (2015), pp. 3235–3283.
[33] M. Wechselberger, *Existence and bifurcation of canards in* $\mathbb{R}^3$ *in the case of a folded node*, SIAM J. Appl. Dyn. Syst., 4 (2005), pp. 101–139.
[34] M. Wechselberger, *Apropos canards*, Trans. Amer. Math. Soc., 364 (2012), pp. 3289–3309.
[35] M. Wechselberger, *Geometric Singular Perturbation Theory Beyond the Standard Form*, Springer, Cham, Switzerland, 2020.
[36] K. C. Wedgwood, K. K. Lin, R. Thul, and S. Coombes, *Phase-amplitude descriptions of neural oscillator models*, J. Math. Neurosci., 3 (2013), 2.
[37] S. Wiggins, *Normally Hyperbolic Invariant Manifolds in Dynamical Systems*, Springer, New York, 1994.
[38] D. Wilson and B. Ermentrout, *Greater accuracy and broadened applicability of phase reduction using isostable coordinates*, J. Math. Biol., 76 (2018), pp. 37–66.